Summary of the Fourth AIAA CFD Drag Prediction Workshop

John C. Vassberg[*], Edward N. Tinoco[†], Mori Mani[‡], Ben Rider[§]
The Boeing Company, Huntington Beach, CA 92647, Seattle, WA, 98124, St. Louis, MO, 63301, USA

Tom Zickuhr[¶], David W. Levy[¶]
Cessna Aircraft Company, Wichita, KS 67218, USA

Olaf P. Brodersen[‖], Bernhard Eisfeld[‖], Simone Crippa[‖]
DLR Institute of Aerodynamics and Flow Technology, 38108 Braunschweig, Germany

Richard A. Wahls[**], Joseph H. Morrison[††]
NASA Langley Research Center, Hampton, VA 23681, USA

Dimitri J. Mavriplis[‡‡]
University of Wyoming, Laramie, WY 82071, USA

Mitsuhiro Murayama[‖]
Japan Aerospace Exploration Agency, Chofu, Tokyo 182-8522, Japan

Abstract

Results from the Fourth AIAA Drag Prediction Workshop (DPW-IV) are summarized. The workshop focused on the prediction of both absolute and differential drag levels for wing-body and wing-body-horizontal-tail configurations that are representative of transonic transport aircraft. Numerical calculations are performed using industry-relevant test cases that include lift-specific flight conditions, trimmed drag polars, downwash variations, dragrises and Reynolds-number effects. Drag, lift and pitching moment predictions from numerous Reynolds-Averaged Navier-Stokes computational fluid dynamics methods are presented. Solutions are performed on structured, unstructured and hybrid grid systems. The structured-grid sets include point-matched multi-block meshes and over-set grid systems. The unstructured and hybrid grid sets are comprised of tetrahedral, pyramid, prismatic, and hexahedral elements. Effort is made to provide a high-quality and parametrically consistent family of grids for each grid type about each configuration under study. The wing-body-horizontal families are comprised of a coarse, medium and fine grid; an optional extra-fine grid augments several of the grid families. These mesh sequences are utilized to determine asymptotic grid-convergence characteristics of the solution sets, and to estimate grid-converged absolute drag levels of the wing-body-horizontal configuration using Richardson extrapolation.

[*]Boeing Technical Fellow, AIAA Fellow
[†]Boeing Technical Fellow (Retired), AIAA Associate Fellow
[‡]Boeing Sr. Technical Fellow, AIAA Associate Fellow
[§]Sr. Engineer, AIAA Member
[¶]Principal Engineer, AIAA Associate Fellow
[‖]Research Engineer, AIAA Member
[**]Assistant Head, Configuration Aerodynamics Branch, AIAA Associate Fellow
[††]Head, Computational AeroSciences Branch, AIAA Senior Member
[‡‡]Professor Mechanical Engineering, AIAA Associate Fellow

Nomenclature

AR	**Wing Aspect Ratio** $= \frac{b^2}{S_{ref}}$
a	**Acoustic Speed**
b	**Wing Span**
BL	**Butt Line Coordinate**
CFD	**Computational Fluid Dynamics**
C_D	**3-D Drag Coefficient** $= \frac{Drag}{q_\infty S_{ref}}$
C_{DP}	**Idealized Profile Drag** $= C_D - \frac{C_L^2}{\pi AR}$
C_{Dpr}	**Pressure Drag Coefficient**
C_{Dsf}	**Skin-Friction Drag Coefficient**
C_L	**Lift Coefficient** $= \frac{Lift}{q_\infty S_{ref}}$
$C_{L\alpha}$	**Lift Curve Slope**
C_M	**Pitching Moment Coefficient**
C_P	**Pressure Coefficient** $= \frac{P-P_\infty}{q_\infty}$
C_{ref}	**Wing Reference Chord** $\simeq$ **MAC**
c_f	**Local Coefficient of Skin Friction**
$count$	**Drag Coefficient Unit** $= 0.0001$
DPW	**Drag Prediction Workshop**
FS	**Fuselage Station Coordinate**
LE	**Wing Leading Edge**
MAC	**Mean Aerodynamic Chord**
N	**Total Number of Grid Points**
P	**Static Pressure**
q	**Dynamic Pressure** $= \frac{1}{2}\rho V^2$
$RANS$	**Reynolds-Averaged Navier-Stokes**
Re	**Reynolds number** $= \frac{\rho_\infty V_\infty C_{ref}}{\mu_\infty}$
S_{ref}	**Reference Area**
SOB	**Side-of-Body**
T	**Temperature**
TE	**Wing Trailing Edge**
V	**Velocity**
WB	**Wing/Body**
$WBNP$	**Wing/Body/Nacelle/Pylon**
WL	**Water Line Coordinate**
Y^+	**Wall Distance** $= Re\sqrt{\frac{c_f}{2}}y$
α	**Angle of Attack**
Δ	**Difference in Quantity**
η	**Fraction of Wing Semi-Span**
μ	**Fluid Viscosity**
ρ	**Fluid Density**
π	3.141592654...
∞	**Signifies Freestream Conditions**

I. Introduction

The AIAA CFD Drag Prediction Workshop (DPW) Series was initiated by a working group of members from the AIAA Applied Aerodynamics Technical Committee. From the onset, the DPW organizing committee defined and has adhered to a set of primary objectives for the DPW Series. These include:

- Assess state-of-the-art computational fluid dynamics (CFD) methods as practical aerodynamic tools for the prediction of forces and moments on industry-relevant geometries, with a focus on absolute drag.
- Provide an impartial international forum for evaluating the effectiveness of CFD Navier-Stokes solvers.
- Promote balanced participation across academia, government labs, and industry.
- Use common public-domain subject geometries, simple enough to permit high-fidelity computations.
- Provide baseline grids to encourage participation and help reduce variability of CFD results.
- Openly discuss and identify areas needing additional research and development.
- Conduct rigorous statistical analyses of CFD results to establish confidence levels in predictions.
- Schedule open-forum sessions to further engage interaction among all interested parties.
- Maintain a public-domain accessible database of geometries, grids, and results.
- Document workshop findings; disseminate this information through publications and presentations.

The first workshop[1] in this series, DPW-I , was held in Anaheim, CA in conjunction with the 19^{th} Applied Aerodynamics Conference of June 2001. The premise of DPW-I was to solicit CFD predictions of a common, industry relevant geometry and assess the results using statistical analysis techniques. Although the focus of the workshop was on drag prediction, lift and pitching moment predictions were also evaluated. The DLR-F4 wing-body configuration was chosen as the subject of DPW-I both because of its simplicity and the availability of publicly released experimental test data.[2] The workshop committee provided a standard set of multi-block structured, overset, and unstructured grids for the DLR-F4 geometry to encourage participation in the workshop and reduce variability in the CFD results. However, participants were also encouraged to construct their own grids using their *best practices* so that learned knowledge concerning grid generation

and drag prediction might be shared[3] among workshop attendees. The test cases were chosen to reflect the interests of industry and included a fixed-C_L single point solution, drag polar, and constant-C_L drag rise data sets. Eighteen participants submitted results, using 14 different CFD codes; many submitted multiple sets of data exercising different options in their codes, e.g., turbulence models and/or different grids. A summary of these results was documented by the DPW-I organizing committee.[4,5] Because of strong participation, DPW-I successfully amassed a CFD data set suitable for statistical analysis.[6,7] However, the results of that analysis were rather disappointing, showing a 270-drag-count spread in the fixed-C_L data, with a 100:1 confidence interval of more than ± 50 drag counts.

Despite the disheartening results of the statistical analysis, DPW-I was a definitive success. It brought together CFD developers and practitioners and focused their efforts on a common problem. It facilitated an exchange of learned best practices and promoted open discussions, identifying areas requiring further research or additional scrutiny. Possibly most significant, it employed statistical methods to objectively assess CFD results. Finally, it reminded the CFD and applied aerodynamics communities that CFD is not yet a fully matured discipline.

In addition to the accomplishments listed above, DPW-I initiated interest in industry-relevant drag predictions that has been sustained through three more workshops, and looks to continue beyond. Several of the participants presented their DPW-I results[8–13] at a well-attended special session of the 2002 AIAA Aerospace Sciences Meeting and Exhibit in Reno, NV. The interest generated by DPW-I naturally led to the planning and organization of the 2^{nd} AIAA Drag Prediction Workshop, DPW-II. The DPW-II organizing committee, recognizing the success of DPW-I, maintained its objectives for DPW-II.

The second workshop[14] was held in Orlando, FL in conjunction with the 21^{st} Applied Aerodynamics Conference of June 2003. For this workshop, the DLR-F6 was chosen as the subject geometry, in both wing-body (WB) and wing-body-nacelle-pylon (WBNP) form. The DPW-II organizing committee worked with DLR and ONERA to make pertinent experimental data available to the public domain. One specific objective of DPW-II was the prediction of the incremental drag associated with nacelle/pylon installation. Although the F6 geometry is similar to that of the F4, its pockets of flow separation at the design condition are more severe; these occur predominantly at the wing/body and wing/pylon juncture regions. Again, this workshop was documented with a summary paper,[15,16] a statistical analysis,[17] an invited reflections paper[18] on the workshop series, and numerous participant papers[19–32] in two special sessions of the 2004 AIAA Aerospace Sciences Meeting in Reno, NV. A conclusion of DPW-II was that the separated flow regions made it difficult to draw meaningful conclusions with respect to grid convergence and drag prediction. During the follow-up open-forum discussions, the CFD community voiced the desire for the organizing committee to include in the third workshop: a) *Blind Test Cases*, and b) *Simpler Geometries*. The request for blind test cases is motivated by an earnest attempt to better establish a measure of the CFD community's capability to predict absolute drag, rather than match it after-the-fact. The request for simpler geometries allows more extensive research in studies of asymptotic grid convergence.

The third workshop[33] was held in San Francisco, CA in conjunction with the 24^{th} Applied Aerodynamics Conference of June 2006. The DLR-F6 WB from DPW-II was retained as a baseline configuration for the DPW-III to provide a bridge between these two workshops. However, to test the hypothesis that the grid-convergence issues of DPW-II were the direct result of the large pockets of flow separation, a new wing-body fairing was designed to eliminate the side-of-body separation. Details of the FX2B fairing design are documented by Vassberg.[34] In addition, to help reduce the wing upper-surface trailing-edge flow separation, a higher Reynolds number was introduced for the WB test cases. These changes in both geometry and flow condition also provided the DPW-III participants a blind test since no test data would be available prior to the workshop. Furthermore, two wing-alone geometries were created to provide workshop participants with simpler configurations on which more extensive grid-convergence studies could be conducted; these wings were designed to not exhibit any appreciable separation at their design conditions. The DPW-III was heavily documented with summary papers,[35–37] a statistical analysis paper,[38] participant papers,[39–42] and a special section of the AIAA Journal of Aircraft, edited by Vassberg.[43–48]

After three workshops, the organizing committee recognized that a recurring theme of the workshop series was related to grid quality and resolution. These issues were documented by Mavriplis.[49]

The fourth workshop[50] was held in San Antonio, TX in conjunction with the 27^{th} Applied Aerodynamics Conference of June 2009. For this workshop, a completely new geometry was developed, called the Common Research Model (CRM). The CRM was developed by NASA's Subsonic Fixed Wing (SFW) Aerodynamics Technical Working Group (TWG), in collaboration with the DPW Organizing Committee. This wing-body-horizontal (with and without nacelle-pylons) configuration is representative of a contemporary high-

performance transonic transport. A detailed description of its development is given by Vassberg.[51]

A particular discriminator of the DPW-IV relative to the first three workshops is in the timing of the availability of wind-tunnel test data on the subject geometries. In DPW-IV, the workshop was held (and all finalized CFD solution sets were provided) several months before any experimental data were collected. Hence, the totality of this workshop is undeniably a set of blind tests. Another advantageous outcome of this collaborative endeavor is that the CRM has been tested in two facilities thus far, and the data from these tests will be made publicly available. The National Transonic Facility (NTF) at NASA Langley tested the CRM during Jan-Feb 2010, and then it was evaluated at the Ames 11-ft wind-tunnel during Mar-Apr 2010. Data from the NTF test, in near final form, will be released to the public domain by Rivers.[52]

DPW-IV had a total of 19 participants submit 29 solution sets for the Common Research Model cases. Balance of participation achieved at this workshop is shown below by the demographics of the DPW-IV.

- USA: 37%, Europe: 37%, Asia/Russia: 26%
- Industry: 25%, Government Labs: 32%, Academia: 11%, Vendors: 32%
- Structured: 31%, Unstructured: 69%
- Returning from DPW-III: 47%, New to DPW-IV: 53%

A tradition of the DPW Series is to follow up the workshop events with dedicated sessions featuring papers at an AIAA conference. The DPW-IV is host to three sessions at the 28^{th} AIAA Applied Aerodynamics Conference which include this paper, the aforementioned experimental data paper by Rivers,[52] a statistical analysis of the DPW-IV results by Morrison,[53] and 14 participant papers.[54–67]

In addition to the publications spawned directly by the DPW Series, the DPW databases have been used elsewhere and continue to be downloaded from the website. Two notable references are by Baker[68] and Salas;[69] both provide independent, rigorous analyses of the grid-sensitivity data generated by the DPW-II. The conclusions of these studies were leveraged by the organizing committee to better construct the test cases for DPW-III & DPW-IV, and although the applications of the test cases still have flaws, the lessons learned from each workshop *have* improved the outcome of subsequent workshops.

When the concept of this workshop series first began to take form in January of 2000, it was impossible then to imagine the magnitude of the cumulative efforts the DPW participants would be willing to invest. Even in retrospect, this is hard to believe. It is a testament that a grass-roots campaign such as this workshop series can accomplish so much. Through the contributions of the DPW participants, the public now has access to a wealth of previously-unavailable CFD data, as well as newly-acquired test data.

Due to the continued success of the DPW Series, spin-off collaborations have yielded high-quality experimental data on the Common Research Model from two test facilities, and additional wind-tunnel data for the DLR-F6 configurations,[70] all of which are now available in the public domain. The DPW Series has established a working model that other workshops are emulating, such as Benek's Shock/Boundary-Layer Workshop appended to the 48^{th} AIAA ASM of January 2010, and the first High-Lift Prediction Workshop (HiLiftPW-I) being held in conjunction with the 28^{th} AIAA Applied Aerodynamics Conference of June 2010.

This paper is organized in the following manner. Section II provides a description of the subject configuration. Section III outlines the test cases of the fourth workshop. Section IV gives a brief description of the family of baseline grids utilized in the workshop. Section V discusses a Richardson extrapolation process used by the present work to develop estimates as the grid resolution approaches the continuum. Section VI provides a sample of pertinent experimental data collected on the CRM at the NTF. Section VII summarizes the collective results of the DPW-IV. Tables of data are embedded within the text closely after first reference, while all figures are appended to the end of this publication.

II. CRM Geometry Description

The baseline wing-body-horizontal (WBH) configuration for DPW-IV is the Common Research Model (CRM). An isometric view of the CRM WBH configuration is shown in Figure 1. The CRM is representative of a contemporary transonic commercial transport designed to cruise at $M = 0.85$ & $C_L = 0.5$ at a nominal altitude of 37,000 ft. However, a couple of features have been designed into this shape solely for the purposes of research & developments. For example, the upper-surface pressure recovery over the outboard wing is intentionally made aggressively adverse over the last 10-15% local chord. The purpose for designing in this

feature is to weaken the health of the upper-surface boundary layer in close proximity to the wing trailing edge (TE). This provides a fairly controlled TE separation, which is a flow phenomena the DPW organizing committee wanted to study in DPW-IV. This pressure architecture also amplifies the differences between the various turbulence models under study, *e.g.* skin-friction drag levels. Another aspect of the CRM design that is not consistent with a real airplane design is related to its spanload. The CRM wing-body spanload is closer to elliptic than typical aircraft designs. Incorporating this feature is motivated by possible future workshops on optimization. For a purely aerodynamic shape optimization, the CRM represents a challenging case in that the optimizers will not be able to extract much improvement by simply manipulating spanload distributions. However, due to the aforementioned TE pressure recovery, the aerodynamic performance of the CRM can be improved by $\sim 2\%$. This level of potential improvement is consistent with that faced by a typical drag-reduction study on an existing aircraft.

Reference quantities and other pertinent information for the CRM are provided below.

S_{ref}	$594,720.0\ in^2 = 4,130\ ft^2$	$[458.89\ m^2]$	
S_{trap}	$576,000.0\ in^2 = 4,000\ ft^2$	$[444.44\ m^2]$	
b	$2,313.5 in = 192.8\ ft$	$[58.765\ m]$	
C_{ref}	$275.800 in = 16.07\ ft$	$[4.8978\ m]$	
AR	9.0		
X_{ref}	$1,325.9\ in$	$[33.68\ m]$	
Y_{ref}	$468.75\ in$	$[11.91\ m]$	
Z_{ref}	$177.95\ in$	$[4.520\ m]$	
$\Lambda_{C/4}$	35.0°		
λ	0.275		

The definition of the horizontal tail of the CRM is comprised of two symmetric airfoil sections, one at the symmetry plane and the other at the horizontal tip. The tip airfoil includes 2.5° of twist. The tail-fuselage intersection line defining the root airfoil section remains sealed against the fuselage as the horizontal rotates about its hinge line. For the downwash study of Case 1b, three horizontal tail settings are used; tail incidences of $iH = [-2^\circ,\ 0^\circ,\ +2^\circ]$. Case 1b also requires a wing/body (no tail) configuration. All other cases of DPW-IV are on the WBH configuration with $iH = 0^\circ$.

For the purpose of future endeavors and experimental investigations, the CRM also includes pylon-nacelles. The nacelles are single-path, flow-through designs with an unforced mass-flow-ratio typical of a commercial transport at cruise conditions. The CRM wing is designed to perform exceptionally well with or without the pylon-nacelle group. For more detailed information on this geometry, see Vassberg.[51]

III. Test Cases

The success of the DPW Series is due in large part to the significant amount of personal time and computing resources invested by the participants of the workshops. In order to keep these individual investments from growing out of control, the organizing committee made optional two of the three test cases for DPW-IV. Participants were only required to conduct Case 1. This manditory test case includes a single-point grid-sensitivity study, and an alpha-sweep on four medium-size grids. Note that a fixed-lift condition requires convergence on α; this in turn adds additional effort. CFD solutions for all test cases are required to represent fully turbulent flow as closely as possible.

The required and optional test cases for DPW-IV are:

Case 1a: Grid-Convergence Study

Fixed-C_L Single-Point Grid-Convergence Study on WBH

- $Mach = 0.85$, $C_L = 0.5 \pm 0.001$, $Re = 5$ million, $iH = 0^\circ$
- Coarse, Medium, Fine, & Extra-Fine Grids (Extra-Fine is optional)

Case 1b: Downwash Study

Drag Polars on Medium WB & WBH Grids

- $Mach = 0.85$, $Re = 5$ million
- $\alpha = [0.0^\circ, 1.0^\circ, 1.5^\circ, 2.0^\circ, 2.5^\circ, 3.0^\circ, 4.0^\circ]$
- Horizontal Tail: *Off* and *On* with $iH = [-2^\circ, 0^\circ, +2^\circ]$

- Trimmed WBH Polar and Lift curves
- Downwash Variation
- Delta Drag Polar: Trimmed WBH − WB

Case 2 (Optional): Mach-Sweep Study

Drag Rises on Medium WBH Grid

- $C_L = [0.40, 0.45, 0.50]$
- $Mach = [0.70, 0.75, 0.80, 0.83, 0.85, 0.86, 0.87]$
- $Re = 5$ million, $iH = 0°$
- Extracted from Polars or C_L converged to ± 0.001

Case 3 (Optional): Reynolds-Number Study

Fixed-C_L Single-Point Solutions on Medium WBH Grid

- $Re = [5$ & $20]$ million
- $Mach = 0.85$, $C_L = 0.5 \pm 0.001$, $iH = 0°$

To collect a consistent set of data from each participant, template datasets were supplied. These templates request lift, drag (broken down by mechanical component), pitching moment, pressure distributions at specified span stations, trailing-edge separation locations, dimensions of the side-of-body separation bubble, grid family and sizes, turbulence model, computing platform and code performance, number of processors used, number of iterations required, etc. These workshops capture an extensive amount of information that serve as a snapshot of the industry capabilities of the time. For example, in the four workshops held thus far, one obvious trend is that the grid size has grown dramatically. The average size of the medium WB meshes in DPW-I through DPW-IV have been 3.2, 5.4, 7.8 and 10.9 million, respectively. This represents a growth rate of $\sim 17\%$ per year during the eight years between DPW-I and DPW-IV.

IV. Baseline Grids

An overview of the baseline grids is provided in this section. However, the details of these grids are not included herein. For more information regarding these grids, please refer to the companion papers[54–67] associated with this summary document. Because of the variation of grid types needed, a set of gridding guidelines, listed below, is established to help facilitate the creation of these grids. The gridding guidelines are provided to persons responsible for generating baseline grids in an attempt to maintain some level of uniformity across all types of meshes. Note that each grid family is required to include a Coarse (C), Medium (M), and Fine (F) grid; adding an optional Extra-Fine (X) grid is also encouraged. Further, the organizing committee decided that the Medium mesh should be representative of current engineering applications of CFD being used to estimate absolute drag levels on similar configurations. For unstructured meshes, the size of the Medium mesh is also a function of the intended flow solver. For example, a cell-centered scheme has about 5.5 times the numbers of unknowns as that of a nodal scheme for a given unstructured tetrahedral mesh, with the ratio being closer to 3.5 for typical hybrid meshes.

Table I provides the grid size for each grid family, configuration, and resolution for Case 1. The types of meshes include multiblock (MB), overset (OS), and unstructured (UN). This table also indicates whether the associated flow solver is based on a nodal (N) or cell (C) centered scheme. These grids range in size from 2.8-to-189.4 million. The average Medium grid sizes for the WBH and WB configurations are 13.3 million and 10.9 million, respectively. Also included in this table is a mapping of the participants who used each grid. The usage key (tag) is described in Table II of Section VII. For example, the Solar grid family (Type UN/N) is comprised of unstructured meshes, appropriately developed for node-based solvers, does not have an extra-fine mesh in its family, and is used by participants C, D, S & T. Note that the average usage of each grid is by 1.6 participants. This low ratio is indicative of the fact that participants have realized that in order to obtain accurate solutions, they prefer to develop grids tailored to their flow solvers.

Gridding Guidelines

- Boundary Layer Region
  - $Y^+ \leq [1,\ \frac{2}{3},\ \frac{4}{9},\ \frac{8}{27}]$ $[C, M, F, X]$
  - $\Delta_1 = 0.000985\, in$, [Dimensional spacing for $Y^+ \sim 1$ and $Re = 5$ million]
  - $\Delta_1 = 0.000273\, in$, [Dimensional spacing for $Y^+ \sim 1$ and $Re = 20$ million]
  - $\Delta_2 = \Delta_1$, [Two cell layers of constant spacing at viscous wall]
  - Growth Rates ≤ 1.25, [Preferably ≤ 1.20]
- Farfield: $\sim 100\ C_{ref}$-lengths away from geometry
- Local Spacings on Medium Grid
  - Chordwise: 0.1% local chord at Wing and Horizontal-Tail Leading & Trailing Edges
  - Spanwise: 0.1% semispan at root & tip of the Wing and Horizontal Tail
  - Cell Size on Fuselage Nose: 2% C_{ref}
- Cells across Wing Trailing-Edge Base: $[8, 12, 16, 24]$ $[C, M, F, X]$
- Grid Family
  - Medium Mesh Representative of Current Engineering Drag Predictions
  - Maintain a Parametric Family of Uniformly-Refined Grids in Sequence
  - Grid Size to Grow $\sim$ 3X for Each Level Refinement [Structured: 1.5X in Each I,J,K Direction]
  - Give Consideration to Multigridable Dimensions on Structured Meshes
  - Target Sizes for CRM WBH: $[3.5, 10, 35, 100]$ million $[C, M, F, X]$

Table I: DPW-IV CRM Grids - Size in Millions.

		WBH ($iH = 0$)				WB	
Family	Type	Extra-Fine	Fine	Medium	Coarse	Medium	Usage
CFSE ICEM Hexa	MB/C	-	36.0	11.3	3.8	11.0	A
Centaur	UN/N	-	-	13.3	-	-	B
Solar	UN/N	-	34.1	11.7	4.1	8.6	C,D,S,T
Gambit/Tgrid	UN/C	-	58.1	21.3	6.2	5.4	E
MEGG3D	UN/N	-	31.3	13.5	5.9	9.8	F
HexaGrid	UN/N	-	36.6	11.1	3.2	9.2	G
GRIDGEN	MB/C	-	30.4	9.0	2.8	8.6	H
VGRID LaRC	UN/N	105.7	36.0	10.3	3.7	8.2	I,K,Z
VGRID Cessna	UN/N	-	35.2	9.9	3.5	8.5	J
Boeing Seattle	MB/C	81.7	47.2	11.0	4.8	10.9	L-O,Y
Boeing HB	OS/N	189.4	56.5	16.9	7.2	12.3	P
ANSYS ICEM Hexa	MB/C	104.3	35.8	10.8	3.5	8.6	R
GRIDZ	MB/C	-	-	15.4	4.4	-	U
Airbus ICEM Hexa	MB/C	104.7	36.7	12.6	4.5	8.8	V
MIME	UN/C	33.9	28.6	16.6	11.5	17.0	W,X
Boeing StL	UN/C	109.4	55.5	22.3	7.1	32.8	2,3
NUMECA	UN/C	-	27.3	14.3	5.2	9.7	4
TriTet	UN/N	-	32.1	10.2	3.2	5.7	5
Average	-	99.7	37.4	13.3	5.0	10.9	1.6

V. Richardson Extrapolation

A Richardson extrapolation can be performed on a pair of data from a grid-convergence trendline to yield an estimate of the continuum value. For the constant-lift grid-convergence study of Case 1a, continuum estimates can be made for α, C_D, C_{Dpr}, C_{Dsf}, or C_M. Let $\mathcal{Y}$ represent any one of these quantities. In the following Lagrange equation, $\mathcal{Y}_{FM}$ & $\mathcal{Y}_{XF}$ are continuum estimates using the Fine/Medium and Extra-Fine/Fine pairs of data, respectively.

$$\mathcal{Y}_{FM} = \frac{\mathcal{X}_M \mathcal{Y}_F - \mathcal{X}_F \mathcal{Y}_M}{\mathcal{X}_M - \mathcal{X}_F}, \quad \mathcal{Y}_{XF} = \frac{\mathcal{X}_F \mathcal{Y}_X - \mathcal{X}_X \mathcal{Y}_F}{\mathcal{X}_F - \mathcal{X}_X}. \tag{1}$$

Here, $\mathcal{X} = N^{-\frac{2}{3}}$, and N is the total number of grid points or cells in the grid system, depending on flow-solver type. The estimated values of $\mathcal{Y}$ in Eqn 1 correspond to an extrapolation to $\mathcal{X} = 0$. As defined, $\mathcal{X}$ is an appropriate parameter for a second-order scheme applied to results on a parametric family of three-dimensional meshes that have been uniformly refined in all three coordinate directions, and provided that the results are within the asymptotic range. Unfortunately, the level to which the uniform-refinement criterion has been achieved varies across the set of baseline grid families. For structured meshes, this requirement can easily be met by uniformly scaling the I, J & K dimensions. For unstructured meshes, the situation is more complicated. One approach is to use a global scaling parameter related to cell sizes, but this technique is difficult to enforce uniformly, and it does not guarantee the mesh connectivity to be self-similar between coarse and fine meshes. Another approach is to subdivide each element into smaller elements, but this can lead to undesirable cell aspect ratios, especially in the finest grid. Nonetheless, Eqn 1 is used herein to generate estimates for grid-converged quantities.

VI. NTF Experimental Data on the CRM

This section includes some pertinent preliminary experimental data for the CRM from NTF Test-197. The process used to determine these data at the lifting condition of $C_L = 0.5$ and $M = 0.85$ is as follows. For each run, alpha-sweeps are linearly-interpolated on C_L to obtain α and C_M. In order to determine C_D, the alpha-sweeps are linearly-interpolated on C_L^2. The aeroelastic effects between the two Reynolds number conditions are minimized by maintaining a constant $\frac{q}{E}$ ratio. Table II provides a summary of these interpolated data, and includes averaged values as well as standard deviations.

Table II: CRM NTF Data: $C_L = 0.5$ & $M = 0.85$.

Run	Config	$Re * 10^{-6}$	C_D	C_M	α
44	WB	5.0	0.02556	-0.06433	2.782°
51	WB	5.0	0.02564	-0.06484	2.781°
53	WB	5.0	0.02561	-0.06479	2.783°
Average	WB	5.0	0.02560	-0.06465	2.782°
σ	-	-	0.00004	0.00028	0.001°
92	WBH+0	5.0	0.02740	+0.03783	3.013°
97	WBH+0	5.0	0.02761	+0.03800	3.021°
99	WBH+0	5.0	0.02753	+0.03771	3.027°
Average	WBH+0	5.0	0.02751	+0.03785	3.020°
σ	-	-	0.00011	0.00015	0.008°
106	WBH+0	19.8	0.02532	+0.03792	2.978°
109	WBH+0	19.8	0.02532	+0.03773	2.981°
111	WBH+0	19.8	0.02520	+0.03796	2.989°
Average	WBH+0	19.8	0.02528	+0.03787	2.983°
σ	-	-	0.00007	0.00012	0.006°

VII. Results

Participants of the DPW-IV were required to provide results on Case 1, which includes a grid-convergence study, and a trimming exercise. To their credit, many participants chose to investigate the optional cases; several even provided multiple datasets on a given case. This section summarizes the data collected on these test cases. These data are then used to estimate absolute drag levels for the CRM. These estimates are made prior to any experimental data being available on any of the configurations. There are twenty-nine submissions for Case 1. The following subsections detail the results for the three test cases.

Case 1: CRM at Cruise Mach

The first test case is focused on the CRM wing-body-horizontal configuration at its cruise Mach number, and comprised of two studies. The first sub-case is a single-point grid-convergence study at the CRM design Mach and lifting condition, but at a representative wind-tunnel Reynolds number. The second sub-case is a down-wash study that includes finding the trimmed drag polar for the CRM WBH configuration. Table III provides the tag label, CFD code, grid type, grid family, turbulence model, and participant organization/name for each block of data submitted.

Table III: DPW-IV Case-1 Submissions.

Tag	Code	Grid Type	Grid Family	Turbulence Model	Submitter
A	NSMB	MB/C	CFSE ICEM Hexa	SST KW	CFS/RUAG Vos
B	TAU	UN/N	Centaur	SA	DLR Brodersen
C	TAU	UN/N	Solar	SA	DLR Brodersen
D	EDGE	UN/N	Solar	EARSM	FOI Eliasson
E	HIFUN	UN/C	Gambit/Tgrid	SA	IIS Ravindra
F	TAS	UN/N	TASmesh	SA mod	JAXA Yamamoto
G	TAS	UN/N	HexaGrid	SA	JAXA Hashimoto
H	UPACS	MB/C	GRIDGEN	SA mod	JAXA Yamamoto
I	FUN3D	UN/N	VGRID LaRC	SA	NASA Lee-Rausch
J	NSU3D	UN/N	VGRID Cessna	SA	Cessna Chaffin
K	NSU3D	UN/N	VGRID LaRC	SA	Cessna Chaffin
L	CFL3D	MB/C	Boeing Seattle	SA	Boeing Rider
M	CFL3D	MB/C	Boeing Seattle	SST KW	Boeing Rider
N	CFL3D	MB/C	Boeing Seattle	SA	Boeing Rider
O	CFL3D	MB/C	Boeing Seattle	SST KW	Boeing Rider
P	OVERFLOW	OS/N	Boeing HB	SA	Boeing Sclafani
R	FLUENT	MB/C	ANSYS ICEM Hexa	SST KW	ANSYS Oswald
S	TAU	UN/N	Solar	SSG/LRR	DLR Brodersen
T	TAU	UN/N	Solar	SST KW	DLR Brodersen
U	FLOWZ	MB/C	GRIDZ	SA	ZEUS-NUMERIX Gupta
V	ELSA	MB/C	Airbus ICEM Hexa	SST KW	Airbus Trapier
W	CFD++	UN/C	MIME	K-Epsilon	Metacomp Goldberg
X	CFD++	UN/C	MIME	SA	Metacomp Goldberg
Y	ELSA	MB/C	Boeing Seattle	SA	ONERA Esquieu
Z	NSU3D	UN/N	VGRID LaRC	SA	UWy Long
2	BCFD	UN/C	Boeing St Louis	SA	Boeing Winkler
3	BCFD	UN/C	Boeing St Louis	SST KW	Boeing Winkler
4	FINE/HEXA	UN/C	NUMECA	SA	NEUMECA Temmerman
5	EDGE	UN/N	TriTet	EARSM	FOI Eliasson

A representative example of the wing pressure distributions at the design condition of $M = 0.85$, $C_L = 0.5$, and wind-tunnel Reynolds number, $Re = 5$ million, is given in Figures 2-3. The span stations of Figure 3 are a subset of those collected in the data submittals forms. Experimental C_P data are available at the $\eta \geq 0.131$ stations of this figure. A full set of the C_P-cut stations on both the wing and horizontal tail are defined in Figure 4. There are 16 cuts on the wing, and 10 cuts on the horizontal tail. The CRM wind-tunnel model includes 9 pressure-tap rows on the wing, and none on the horizontal tail, also shown in Figure 4.

Case 1a: Fixed-C_L Single-Point Grid-Convergence Study

Figure 5 provides grid-convergence trendlines for total drag at the single-point fixed-C_L condition; $C_L = 0.5$. In this figure, side-by-side comparison plots are shown; unstructured-mesh data is captured in the left plot and structured-mesh data on the right. The curves of these plots are labeled with the tag letter given in Table III. Figure 5 includes all of the total-drag data from all submissions. Note that some data fall beyond the range of these plots. These data are also organized by turbulence model, as given by curve type. The following description of curve types holds for Figures 5, 7, 9, 11, and 13. Solid black lines indicate that the results are generated using a version of the Spalart-Almaras (SA) model. Dashed red lines infer Menter's SST model. Chain-dot green lines signify the EARSM model. Long-dash-double-dot blue lines represent the SSG/LRR model. Long-dash aqua lines capture the k-epsilon model. All structured-grid results are either based on the SA or the SST models. With only one exception, the structured-grid results are converging to a total-drag level in the neighborhood of 270 counts. The set of unstructured-mesh data includes all 5 turbulence models. Although this group exhibits more scatter than that of the structured-mesh results, the center of its grid-convergence band is also about 270 counts.

Recall that the Medium-mesh results represent current engineering practices. Here, the Medium-mesh grid-factor, $N^{-\frac{2}{3}}$, falls within the range $[1, 2] * 10^{-5}$. Hence, the range of the total-drag scatter for current engineering practices is on the order of 40 counts, as indicated by Figure 5. A companion paper by Morrison[53] will address this scatter and better quantify confidence levels through a rigorous statistical analysis.

Table IV provides continuum estimates for α, C_D, C_{Dpr}, C_{Dsf}, and C_M for each of the data blocks, where applicable, using Eqn 1. Data-block B only provided data for one mesh level, and data-block W only provided data for total drag, hence some continuum estimates are not possible. Appended to this table is a simple statistical analysis of the continuum estimates. For example, the standard deviation, σ, for C_D is 0.00081 or 8.1 counts. Note that this statistical analysis omits the unavailable estimates from data blocks B & W, as well as the results of data block U, which is clearly an outlier; all other data are included.

It is interesting to note that the standard deviation of the total drag is only 8.1 counts, while that for its components of pressure and skin-friction are 8.3 counts and 4.7 counts, respectively. If the components are fully independent of each other, one would expect the standard deviation of the whole to be closer to the square-root of the sum of the squares of the parts, *i.e.*, $\sqrt{8.3^2 + 4.7^2} = 9.5$. Hence, the pressure and skin-friction components of drag are related. Of course this is already known. As a boundary layer weakens, typically, pressure drag increases, while skin-friction reduces. This compensating effect is reflected in the statistical analysis.

Figure 6 illustrates the distribution of continuum estimates for total drag. This figure includes three horizontal black lines which depict the average and $\pm\sigma$ levels. Here, $\bar{C}_D = 270.1$ counts and $\sigma = 8.1$ counts. The green horizontal line depicts the average of NTF experimental data from Table II, $\bar{C}_D = 0.02751$. Hence, the experimental results are 5 counts higher than the average of the CFD continuum values. The CFD computations were all run fully turbulent, whereas the experiments have short laminar runs upto the transition strips. A laminar run will reduce drag, while the transition strip itself will increase drag. These opposing effects are of the same order of magnitude. However, the turbulence levels in CFD simulations tend to rise gradually; this is not like real flows which transition rapidly. Hence, while the experimental data may be somewhat self correcting, the CFD simulations are not, and it is unclear how much this may affect drag.

Figures 7-8 provide trendlines and the distribution of continuum estimates for pressure drag, C_{Dpr}, respectively. Again the scatter band of the unstructured-mesh data is larger than that of the structured-mesh results. By visual inspection, the center of each band is approaching 146 ± 1 counts in the continuum, with the unstructured-mesh trend about 2 counts higher than that of the structured-mesh. The statistical analysis of Table IV found $\bar{C}_{Dpr} = 147.1$ counts, and its standard deviation $\sigma = 8.3$ counts. As in Figure 6, $\bar{C}_{Dpr}$ and $\bar{C}_{Dpr} \pm \sigma$ levels are included for reference in Figure 8.

Table IV: Case 1a CRM Data Extrapolated to Continuum.

Tag	α	C_D	C_{Dpr}	C_{Dsf}	C_M
A	2.441	0.02884	0.01659	0.01225	-0.02163
B	-	-	-	-	-
C	2.279	0.02696	0.01426	0.01271	-0.04078
D	2.440	0.02783	0.01500	0.01283	-0.03226
E	2.290	0.02619	0.01448	0.01170	-0.03933
F	2.312	0.02707	0.01444	0.01265	-0.03767
G	2.399	0.02674	0.01486	0.01188	-0.03557
H	2.311	0.02692	0.01425	0.01266	-0.03817
I	2.366	0.02686	0.01461	0.01223	-0.03543
J	2.026	0.02475	0.01283	0.01193	-0.06184
K	2.394	0.02652	0.01430	0.01222	-0.02082
L	2.340	0.02747	0.01463	0.01284	-0.04310
M	2.413	0.02730	0.01492	0.01241	-0.03680
N	2.341	0.02731	0.01453	0.01278	-0.04480
O	2.408	0.02719	0.01481	0.01236	-0.03720
P	2.286	0.02650	0.01397	0.01254	-0.03926
R	2.369	0.02701	0.01482	0.01218	-0.03913
S	2.382	0.02669	0.01478	0.01192	-0.03130
T	2.386	0.02711	0.01479	0.01206	-0.02850
U	2.924	0.03994	0.01875	0.02118	-2.39339
V	2.323	0.02737	0.01450	0.01293	-0.03948
W	-	0.02597	-	-	-
X	2.239	0.02588	0.01435	0.01153	-0.10283
Y	2.380	0.02729	0.01456	0.01273	-0.04180
Z	2.434	0.02682	0.01462	0.01219	-0.02195
2	2.333	0.02687	0.01420	0.01267	-0.04138
3	2.411	0.02725	0.01474	0.01251	-0.03642
4	2.113	0.02849	0.01750	0.01099	-0.06497
5	2.425	0.02804	0.01519	0.01286	-0.03417

Statistical Analysis of Continuum Data.

Average	2.340	0.02701	0.01471	0.01233	-0.04025
σ	0.097	0.00081	0.00083	0.00047	0.01612
$Avg + \sigma$	2.437	0.02781	0.01554	0.01280	-0.02413
$Avg - \sigma$	2.243	0.02620	0.01389	0.01186	-0.05638
$\frac{\sigma}{\lvert Avg \rvert}$	0.041	0.300	0.056	0.038	0.400

Note: Omits data-blocks B, U & most of W.

Figures 9-10 illustrate the trendlines of skin-friction drag, and corresponding Richardson extrapolated estimates, respectively. In this case, the scatter bands between the unstructured-mesh and structured-mesh results are very comparable in that they are both fairly flat and relatively narrow. By the eye, the center of the unstructured-mesh band is tending towards 122 counts, while that of the structured-mesh is headed to about 125 counts. Recall that the center of the unstructured-mesh pressure-drag band of Figure 7 is slightly higher ($\sim$ 2 counts) than that of the structured-mesh. Hence, Figures 7 & 9 reinforce the aforementioned compensating effect between the components of total drag. For reference, Figure 10 includes the levels of

$\bar{C}_{Dsf} = 123.3$ and $\bar{C}_{Dsf} \pm \sigma$, where $\sigma = 4.7$ counts.

Figures 11-12 depict grid-convergence characteristics for pitching moment. Figure 12 includes the three similar statistical levels, where $\bar{C}_M = -0.04025$ and $\sigma = 0.01612$. Unlike the trends of the various drags, the scatter band of pitching moment appears to be expanding in size with higher grid resolution! However, if the data blocks that fall outside the $\pm\sigma$ range are ignored for the moment, the scatter band for the remaining solutions contracts instead. Whether or not it is appropriate to view the situation in this manner, is another matter. Nonetheless, it is an interesting observation. The NTF pitching-moment data that correspond to this flow condition gives $\bar{C}_M = +0.03785$, which is significantly different than the CFD results of DPW-IV. Experience tells us that a good part of the difference is due to the interference effects of the upper-swept-strut/sting mounting system, which induces a nose-up pitching moment on the model. As previously mentioned, a tare & interference study was outside the scope of the initial wind-tunnel testing. Further, a computational assessment of this type was not part of DPW-IV.

Our final grid-convergence trends are for angle-of-attack, α, which are given in Figures 13-14. (A typo in data block Y on the fine mesh was corrected.) Here, both unstructured-mesh and structured-mesh results are tending towards $\alpha \sim 2.35°$ in the continuum. Both scatter bands are flat and contract with increasing grid resolution. Figure 14 gives the distribution of continuum estimates for α, and includes levels of $\bar{\alpha} = 2.34°$ and $\bar{\alpha} \pm \sigma$, where $\sigma = 0.097°$. NTF data gives $\bar{\alpha} = 3.02°$, a shift of $\Delta\alpha = 0.68°$ relative to the CFD predictions.

A final note regarding the data of the grid-convergence study: a requirement of this study is that each solution was to be converged in lift to $C_L = 0.5 \pm 0.001$. Although the data-submittal forms requested the value of C_L to five decimal places, several data blocks were submitted with the precise value of $C_L = 0.5$ instead of the actual integrated result. As a consequence, no attempt has been made to correct drag, moment, or angle-of-attack in the data presented herein.

Case 1b: Downwash Study on Medium Grids

The second mandatory sub-case of Case 1 is based on a downwash study in aircraft design. Here, four alpha-sweeps of the CRM are performed, three on the WBH configuration at different horizontal-tail settings, and one without the tail on the WB configuration. The tail settings are $iH = [-2°, 0°, +2°]$. The three WBH polars provide sufficient information to reconstruct a *trimmed* drag polar, and *trimmed* lift curve. In this study, the CRM WBH is being trimmed at its $Xref$, hence, C_M is set to zero at all lifting conditions. In order to determine the average downwash on the horizontal tail, the WB lift curve is matched for the WBH configuration by adjusting (interpolating) the tail setting, iH, for each angle-of-attack. These data are also used to develop trim-drag penalty by comparing trimmed-WBH and WB polars. A select subset of these data will be presented here.

Figure 15 provides the idealized profile drag polar for the CRM WBH with $iH = 0°$. Although not shown here, the $iH = +2°$ WBH polars are about 5 counts lower drag than the $iH = 0°$ polars, and the $iH = -2°$ polars are about 20 counts higher drag than the $iH = 0°$ polars. These deltas are fairly consistent with those of the NTF data.
Idealized profile drag is defined as:

$$C_{DP} \equiv C_D - \frac{C_L^2}{\pi AR}. \tag{2}$$

Plotting C_{DP} instead of C_D can be very useful as its variation with C_L is significantly diminished, and therefore, the scale of the plot can be greatly increased. In Figure 15, the full band of visible drag levels at low C_L conditions is about 35 counts, while at $C_L = 0.5$ it grows to about 45 counts. (There is one outlying polar that falls off this plot, far to the right side.) While there is some indication of a trend in drag level for different turbulence models, readers are cautioned that there is not a rich enough sample to isolate turbulence model as the cause. Other factors such as grid type can be involved.

Figure 16 depicts the lift curves for the CRM WBH with $iH = 0°$ and WB configurations. Note that the scatter of data is similar between WBH and WB configurations. The lift-curve slope for the WBH is $C_{L\alpha} \sim 0.149$ per degree, and for the WB is $C_{L\alpha} \sim 0.139$ per degree. The alpha shift at $C_L = 0.5$ is about $0.1°$ lower for the WB configuration than it is for the WBH with $iH = 0°$. Unanimously, the data concur that the lift-curve break occurs between 3°-4° for both WBH and WB configurations.

It is noted that α is a *derived* quantity in the experimental data. There are significant effects due to mounting system, walls, and aeroelastics. For a model like the CRM, these effects can induce a change of $0.3°$ to $0.4°$. Although some corrections have been applied to the NTF data, to accurately assess these

effects, an expensive tare & interference test is required, and this is beyond the scope of the initial CRM wind-tunnel test campaign.

Figure 17 illustrates the pitching-moment curves for the WBH at the three tail settings, as well as for the WB configuration. Note that C_M is plotted negative to the right per aerodynamic convention. The group of WBH with $iH = -2^\circ$ curves is to the left of this plot, while the $iH = 0^\circ$ set is near the center, and the $iH = +2^\circ$ cluster at the far right. The WB group falls between the $iH = 0^\circ$ and $iH = +2^\circ$ sets. The stability ($-\frac{\delta C_M}{\delta C_L}$) of the WBH curves at $C_L = 0.5$ is approximately 0.271, and that of the WB is about 0.123. These slopes compare very well with the NTF data, which break unstable at $C_L \sim 0.56$. Also at $C_L = 0.5$, the $iH = 0^\circ$ group has $C_M \sim -0.045$ and the $iH = -2^\circ$ set has $C_M \sim +0.097$. Hence, in order to trim the WBH, the tail should be set to $iH \sim -0.63^\circ$. The C_M curves also break between 3°-4° for both WBH and WB configurations. Most of these curves break to the left (unstable), however a few break to the right (even more stable). It is likely that the curves breaking unstable are associated with an outboard-wing stall, while those breaking even more stable are probably experiencing a rapid expanse of the side-of-body (SOB) separation bubble. Nonetheless, up to the pitch break, the CFD results match the slope of the NTF data quite reasonably.

In the case of both the NTF and Ames 11-ft wind-tunnel tests, the CRM model is supported by an upper-swept-strut/sting combination. The upper-swept-strut (blade) resembles a vertical fin. The presence of this mounting system primarily affects the flow over the aft end of the fuselage, which can significantly affect the absolute value of pitching moment. This is particularly true when the model includes a horizontal tail. The blade-sting induces a downward flow on the horizontal, which increases the nose-up pitching moment. Furthermore, an increase in downwash affects the drag of a lifting tail. Again, to accurately correct these effects, an expensive tare & interference study is required.

Figure 18 provides the trimmed polars of idealized profile drag as well as the tail setting required to trim the WBH as a function of lift. (The raw data from block E were re-trimmed by the authors.) Most of the trimmed polars fall within a 20 count band. The spread of iH required to trim is about 0.5°.

Figure 19 illustrates the length of wing trailing-edge separation on the wing at $M = 0.85$, $C_L = 0.5$ and $Re = 5$ million. The consensus of the CFD results is that the $\eta = 0.73$ station exhibits the largest amount of TE separation, however, the amount varies from about 1-3% local chord.

Case 2: Mach-Sweep Study (Optional)

The second test case of the DPW-IV is a Mach-sweep study on a medium mesh. As this case is optional, only a dozen participants conducted this investigation. In order to be able to construct drag-rise curves, participants computed drag levels at seven Mach numbers and three lifting conditions. Some participants chose to converge their solutions to the specified C_L conditions, while others performed alpha-sweeps at each Mach number, and then, interpolated their polars to determine C_D at the three C_L conditions. Figure 20 illustrates the computed drag-rise curves, with unstructured-mesh results on the left and structured-mesh data on the right. All unstructured-mesh data submitted in Case 2 are based on the SA turbulence model, while the structured-mesh results are comprised of SA and SST models. For the purpose of this discussion, we define drag-divergence Mach number, M_{dd}, as the speed at which the total drag is 20 counts greater than it is at $M = 0.70$. With only one exception, all of these results indicate that $M_{dd} \sim 0.85$ for the CRM WBH; this is consistent with the cruise design point of the CRM.

Case 3: Reynolds-number Study (Optional)

The third test case of the DPW-IV is a Reynolds-number study about the CRM WBH configuration with $iH = 0^\circ$. The freestream conditions are $M = 0.85$, $C_L = 0.5$, and $Re = [5, 20]$ million. However, in this exercise, another Medium grid is developed such that equivalent Y^+ spacings at the viscous surfaces are maintained between Reynolds-number conditions. Figure 21 shows the results of DPW-IV, segregated by turbulence-model type. Here, the SA results give a shift in total drag of about −31 counts, while the SST data indicate −35 counts. The NTF data shows a shift of $\Delta C_D = -22.3$ counts. The shifts in pitching moment for SA, SST, and NTF are about −0.005, −0.006, and +0.00002, respectively. The corresponding shifts in angle-of-attack are −0.19°, −0.23°, and −0.038°. The discrepancies between CFD predictions and NTF data of deltas due to Reynolds-number effects are quite significant. Further experimental and computational work may be required to better understand these differences.

Additional Post-Workshop Investigations

The DPW-IV has generated much interest in continuing studies. For example, on-going collaborative efforts between NASA and Boeing, focused on overset meshes, will be documented by Sclafani[54] which include code-to-code comparisons on common grids, as well as extending the grid-convergence studies to mesh sizes of about 2.5 billion nodes.

General Observation

A general observation, after reviewing all of the results, is that there is a set of CFD codes whose members all seem to agree relatively well with each other, and do so over all of the test cases spanning the entire DPW Series. Most noteworthy about this core set of codes is that it is comprised of flow solvers that are based on all types of grids. Hence, several structured, unstructured, and hybrid mesh solvers have matured sufficiently to be useful CFD tools for accurate drag predictions.

VIII. Conclusions

Results from the Fourth AIAA Drag Prediction Workshop (DPW-IV) are summarized. This workshop focused on the prediction of drag for wing-body-horizontal configurations representative of transonic transport aircraft. Numerical calculations are performed using industry-relevant test cases. Numerous Reynolds-Averaged Navier-Stokes CFD results on fully-turbulent flows are provided. These solutions are performed on structured, unstructured, and hybrid grid systems. The structured grid sets include point-matched multi-block meshes and over-set grid systems. The unstructured and hybrid grid sets are comprised of tetrahedral, pyramid, prismatic, and hexahedral elements. Effort is made to provide a high-quality and parametrically consistent family of grids for each grid type for the baseline wing-body-horizontal configuration under study. The wing-body-horizontal families are comprised of a coarse, medium, and fine grid; some are augmented with an optional extra-fine mesh. These mesh sequences are utilized to help determine how provided flow solutions fair with respect to asymptotic grid convergence, and are used to estimate an absolute drag of each configuration via Richardson extrapolation.

The DPW Series has provided a very broad view of the state-of-the-art of CFD applications within the industry, much more so than that which can be garnered by an isolated study. In fact, by reviewing in isolation any one of the DPW-IV's individual data blocks, one may arrive at different conclusions than those presented herein. For example, a typical publication may show how successful a CFD solution matches test data. By combining a large set of solutions from many sources around the world, this workshop clearly shows that there remains room for improvement. However, this conclusion is tempered by an observation that there exists a core set of CFD methods that consistently agree with each other in general, and do so on all test cases spanning the entire workshop series. Most noteworthy about this core set of solvers is that these methods are based on all grid types.

Through the data compiled by this workshop, it is obvious that several problematic issues continue to persist in the processes used for accurate drag prediction. Generating a consistent set of grids for the purpose of grid-convergence studies remains a challenge, especially for unstructured meshes. However, on a good note, the skin-friction predictions of the aggregate data blocks are well behaved and form relatively tight groupings.

IX. Acknowledgments

The authors thank the AIAA Applied Aerodynamics Technical Committee for sponsoring the Drag Prediction Workshop Series. We also thank our respective organizations for their continued support in this endeavor. A special thanks is extended to the participants of DPW-IV, for without their contributions, this workshop would not have been possible. Melissa Rivers provided NTF CRM experimental data in advance so they could be included herein. Finally, the planning of these workshops throughout the duration of the series has been conducted by a substantial number of dedicated individuals. Members of the aggregate organizing committees include: Shreekant Agrawal, Olaf Brodersen, Simone Crippa, Bob Dowgwillo, Bernhard Eisfeld, Jean Luc Godard, Mike Hemsch, Steve Klausmeyer, Kelly Laflin, Dave Levy, Mori Mani, Rick Matus, Dimitri Mavriplis, Joe Morrison, Bas Oskam, Shahyar Pirzadeh, Mark Rakowitz, Ben Rider, Ed Tinoco, John Vassberg, Rich Wahls, and Tom Zickuhr.

References

[1]1^{st} AIAA CFD Drag Prediction Workshop. http://aaac.larc.nasa.gov/tsab/cfdlarc/aiaa−dpw/Workshop1/workshop1.html, dpw@cessna.textron.com, Anaheim, CA, June 2001.

[2]G. Redeker. DLR-F4 wing-body configuration. In *A Selection of Experimental Test Cases for the Validation of CFD Codes*, number *AR-303*, pages B4.1–B4.21. AGARD, August 1994.

[3]J. C. Vassberg, M. A. DeHaan, and A. J. Sclafani. Grid generation requirements for accurate drag predictions based on OVERFLOW calculations. *AIAA Paper 2003-4124*, 16^{th} AIAA Computational Fluid Dynamics Conference, Orlando, FL, June 2003.

[4]D. W. Levy, J. C. Vassberg, R. A. Wahls, T. Zickuhr, S. Agrawal, S. Pirzadeh, and M. J. Hemsch. Summary of data from the first AIAA CFD Drag Prediction Workshop. *AIAA paper 2002-0841*, 40^{th} AIAA Aerospace Sciences Meeting & Exhibit, Reno, NV, January 2002.

[5]D. W. Levy, J. C. Vassberg, R. A. Wahls, T. Zickuhr, S. Agrawal, S. Pirzadeh, and M. J. Hemsch. Summary of data from the first AIAA CFD Drag Prediction Workshop. *AIAA Journal of Aircraft*, 40(5):875–882, Sep–Oct 2003.

[6]M. J. Hemsch. Statistical analysis of CFD solutions from the Drag Prediction Workshop. *AIAA paper 2002-0842*, 40^{th} AIAA Aerospace Sciences Meeting & Exhibit, Reno, NV, January 2002.

[7]M. Hemsch. Statistical analysis of CFD solutions from the Drag Prediction Workshops. In *CFD-based Aircraft Drag Prediction and Reduction*, Hampton, VA, November 2003. von Karman Institue Lecture Series.

[8]M. Rakowitz, B. Eisfeld, D. Schwamborn, and M. Sutcliffe. Structured and unstructured computations on the DLR-F4 wing-body configuration. *AIAA paper 2002-0837*, 40^{th} AIAA Aerospace Sciences Meeting & Exhibit, Reno, NV, January 2002.

[9]M. Rakowitz, B. Eisfeld, D. Schwamborn, and M. Sutcliffe. Structured and unstructured computations on the DLR-F4 wing-body configuration. *AIAA Journal of Aircraft*, 40(2):256–264, 2003.

[10]D. J. Mavriplis and D. W. Levy. Transonic drag predictions using an unstructured multigrid solver. *AIAA paper 2002-0838*, 40^{th} AIAA Aerospace Sciences Meeting & Exhibit, Reno, NV, January 2002.

[11]D. J. Mavriplis and D. W. Levy. Transonic drag predictions using an unstructured multigrid solver. *AIAA Journal of Aircraft*, 42(4):887–893, 2005.

[12]S. Z. Pirzadeh and N. T. Frink. Assessment of the unstructured grid software TetrUSS for drag prediction of the DLR-F4 configuration. *AIAA paper 2002-0839*, 40^{th} AIAA Aerospace Sciences Meeting & Exhibit, Reno, NV, January 2002.

[13]J. C. Vassberg, P. G. Buning, and C. L. Rumsey. Drag prediction for the DLR-F4 wing/body using OVERFLOW and CFL-3D on an overset mesh. *AIAA Paper 2002-0840*, 40^{th} AIAA Aerospace Sciences Meeting & Exhibit, Reno, NV, January 2002.

[14]2^{nd} AIAA CFD Drag Prediction Workshop. http://aaac.larc.nasa.gov/tsab/cfdlarc/aiaa−dpw/Workshop2/workshop2.html, dpw@cessna.textron.com, Orlando, FL, June 2003.

[15]K. R. Laflin, J. C. Vassberg, R. A. Wahls, J. H. Morrison, O. Brodersen, M. Rakowitz, E. N. Tinoco, and J. Godard. Summary of data from the second AIAA CFD Drag Prediction Workshop. *AIAA Paper 2004-0555*, 42^{nd} AIAA Aerospace Sciences Meeting and Exhibit, Reno, NV, January 2004.

[16]K. R. Laflin, J. C. Vassberg, R. A. Wahls, J. H. Morrison, O. Brodersen, M. Rakowitz, E. N. Tinoco, and J. Godard. Summary of data from the second AIAA CFD Drag Prediction Workshop. *AIAA Journal of Aircraft*, 42(5):1165–1178, 2005.

[17]M. Hemsch and J. Morrison. Statistical analysis of CFD solutions from 2^{nd} Drag Prediction Workshop. *AIAA Paper 2004-0556*, 42^{nd} AIAA Aerospace Sciences Meeting and Exhibit, Reno, NV, January 2004.

[18]N. Pfeiffer. Reflections on the second Drag Prediction Workshop. *AIAA Paper 2004-0557*, 42^{nd} AIAA Aerospace Sciences Meeting and Exhibit, Reno, NV, January 2004.

[19]O. Brodersen, M. Rakowitz, S. Amant, P. Larrieu, D. Destarac, and M. Sutcliffe. Airbus, ONERA, and DLR results from the 2^{nd} AIAA CFD Drag Prediction Workshop. *AIAA Paper 2004-0391*, 42^{nd} AIAA Aerospace Sciences Meeting and Exhibit, Reno, NV, January 2004.

[20]O. P. Brodersen, M. Rakowitz, S. Amant, P. Larrieu, D. Destarac, and M. Suttcliffe. Airbus, ONERA and DLR results from the second AIAA Drag Prediction Workshop. *AIAA Journal of Aircraft*, 42(4):932–940, 2005.

[21]R. B. Langtry, M. Kuntz, and F. Menter. Drag prediction of engine-airframe interference effects with CFX-5. *AIAA Paper 2004-0392*, 42^{nd} AIAA Aerospace Sciences Meeting and Exhibit, Reno, NV, January 2004.

[22]R. B. Langtry, M. Kuntz, and F. Menter. Drag prediction of engine-airframe interference effects with CFX-5. *AIAA Journal of Aircraft*, 42(6):1523–1529, 2005.

[23]A. J. Sclafani, M. A. DeHaan, and J. C. Vassberg. OVERFLOW drag predictions for the DLR-F6 transport configuration: A DPW-II case study. *AIAA Paper 2004-0393*, 42^{nd} AIAA Aerospace Sciences Meeting and Exhibit, Reno, NV, January 2004.

[24]C. Rumsey, M. Rivers, and J. Morrison. Study of CFD variations on transport configurations from the 2^{nd} AIAA Drag Prediction Workshop. *AIAA Paper 2004-0394*, 42^{nd} AIAA Aerospace Sciences Meeting and Exhibit, Reno, NV, January 2004.

[25]K. Wutzler. Aircraft drag prediction using Cobalt. *AIAA Paper 2004-0395*, 42^{nd} AIAA Aerospace Sciences Meeting and Exhibit, Reno, NV, January 2004.

[26]G. May, E. van der Weide, A. Jameson, and S. Shankaran. Drag prediction of the DLR-F6 configuration. *AIAA Paper 2004-0396*, 42^{nd} AIAA Aerospace Sciences Meeting and Exhibit, Reno, NV, January 2004.

[27]Y. Kim, S. Park, and J. Kwon. Drag prediction of DLR-F6 using the turbulent Navier-Stokes calculations with multigrid. *AIAA Paper 2004-0397*, 42^{nd} AIAA Aerospace Sciences Meeting and Exhibit, Reno, NV, January 2004.

[28]K. Yamamoto, A. Ochi, E. Shima, and R. Takaki. CFD sensitivity to drag prediction on DLR-F6 configuration by structured method and unstructured method. *AIAA Paper 2004-0398*, 42^{nd} AIAA Aerospace Sciences Meeting and Exhibit, Reno, NV, January 2004.

[29]E. Tinoco and T. Su. Drag prediction with the Zeus/CFL3D system. *AIAA Paper 2004-0552*, 42^{nd} AIAA Aerospace Sciences Meeting and Exhibit, Reno, NV, January 2004.

[30]S. Klausmeyer. Drag, lift, and moment estimates for transonic aircraft using the Navier-Stokes equations. *AIAA Paper 2004-0553*, 42^{nd} AIAA Aerospace Sciences Meeting and Exhibit, Reno, NV, January 2004.

[31]E. Lee-Rausch, N. Frink, W. Milholen, and D. Mavriplis. Transonic drag prediction using unstructured grid solvers. *AIAA Paper 2004-0554*, 42^{nd} AIAA Aerospace Sciences Meeting and Exhibit, Reno, NV, January 2004.

[32]E. Lee-Rausch, P. Buning, D. Mavriplis, J. Morrison, M. Park, S. Rivers, and C. Rumsey. CFD sensitivity analysis of a Drag Prediction Workshop wing/body transport. *AIAA Paper 2003-3400*, 41^{st} AIAA Applied Aerodynamics Conference, Orlando, FL, June 2003.

[33]3^{rd} AIAA CFD Drag Prediction Workshop. http://aaac.larc.nasa.gov/tsab/cfdlarc/aiaa−dpw/Workshop3/workshop3.html, dpw@cessna.textron.com, San Francisco, CA, June 2006.

[34]J. C. Vassberg, A. J. Sclafani, and M. A. DeHaan. A wing-body fairing design for the DLR-F6 model: a DPW-III case study. *AIAA Paper 2005-4730*, AIAA 23^{rd} Applied Aerodynamics Conference, Toronto, Canada, June 2005.

[35]J. C. Vassberg, E. N. Tinoco, M. Mani, O. P. Brodersen, B. Eisfeld, R. A. Wahls, J. H. Morrison, T. Zickuhr, K. R. Laflin, and D. J. Mavriplis. Summary of the third AIAA CFD Drag Prediction Workshop. *AIAA Paper 2007-0260*, 45^{th} AIAA Aerospace Sciences Meeting and Exhibit, Reno, NV, January 2007.

[36]J. C. Vassberg, E. N. Tinoco, M. Mani, O. P. Brodersen, B. Eisfeld, R. A. Wahls, J. H. Morrison, T. Zickuhr, K. R. Laflin, and D. J. Mavriplis. Abridged summary of the third AIAA CFD Drag Prediction Workshop. *AIAA Journal of Aircraft*, 45(3):781–798, May–June 2008.

[37]J. C. Vassberg, E. N. Tinoco, M. Mani, O. P. Brodersen, B. Eisfeld, R. A. Wahls, J. H. Morrison, T. Zickuhr, K. R. Laflin, and D. J. Mavriplis. Summary of DLR-F6 wing-body data from the third AIAA CFD Drag Prediction Workshop. *RTO AVT-147 Paper 57*, RTO AVT-147 Symposium, Athens, Greece, December 2007.

[38]J. H. Morrison and M. J. Hemsch. Statistical analysis of CFD solutions from the third AIAA Drag Prediction Workshop. *AIAA Paper 2007-0254*, 45^{th} AIAA Aerospace Sciences Meeting and Exhibit, Reno, NV, January 2007.

[39]E. N. Tinoco, C. Winkler, M. Mani, and V. Venkatakrishnan. Structured and unstructured solvers for the 3^{rd} CFD Drag Prediction Workshop. *AIAA Paper 2007-0255*, 45^{th} AIAA Aerospace Sciences Meeting and Exhibit, Reno, NV, January 2007.

[40]D. J. Mavriplis. Results from the 3^{rd} Drag Prediction Workshop using the NSU3D unstructured mesh solver. *AIAA Paper 2007-0256*, 45^{th} AIAA Aerospace Sciences Meeting and Exhibit, Reno, NV, January 2007.

[41]A. J. Sclafani, J. C. Vassberg, N. A. Harrison, M. A. DeHaan, C. L. Rumsey, S. M. Rivers, and J. H. Morrison. Drag predictions for the DLR-F6 wing/body and DPW wings using CFL3D and OVERFLOW on an overset mesh. *AIAA Paper 2007-0257*, 45^{th} AIAA Aerospace Sciences Meeting and Exhibit, Reno, NV, January 2007.

[42]O. Brodersen, B. Eisfeld, J. Raddatz, and P. Frohnapfel. DLR results from the third AIAA CFD Drag Prediction Workshop. *AIAA Paper 2007-0259*, 45^{th} AIAA Aerospace Sciences Meeting and Exhibit, Reno, NV, January 2007.

[43]E. N. Tinoco, V. Venkatakrishnan, C. Winkler, and M. Mani. Structured and unstructured solvers for the third AIAA CFD Drag Prediction Workshop. *AIAA Journal of Aircraft*, 45(3):738–749, May–June 2008.

[44]D. J. Mavriplis. Third Drag Prediction Workshop results using NSU3D unstructured mesh solver. *AIAA Journal of Aircraft*, 45(3):750–761, May–June 2008.

[45]A. J. Sclafani, J. C. Vassberg, N. A. Harrison, C. L. Rumsey, S. M. Rivers, and J. H. Morrison. CFL3D / OVERFLOW results for DLR-F6 wing/body and Drag Prediction Workshop wing. *AIAA Journal of Aircraft*, 45(3):762–780, May–June 2008.

[46]M. Murayama and K. Yamamoto. Comparison study of drag prediction by structured and unstructured mesh method. *AIAA Journal of Aircraft*, 45(3):799–822, May–June 2008.

[47]O. Brodersen, B. Eisfeld, J. Raddatz, and P. Frohnapfel. DLR results from the third AIAA Computational Fluid Dynamics Drag Prediction Workshop. *AIAA Journal of Aircraft*, 45(3):823–836, May–June 2008.

[48]P. Eliasson and S.-H. Peng. Drag prediction for the DLR-F6 wing-body configuration using the Edge solver. *AIAA Journal of Aircraft*, 45(3):837–847, May–June 2008.

[49]D. J. Mavriplis, J. C. Vassberg, E. N. Tinoco, M. Mani, O. P. Brodersen, B. Eisfeld, R. H. Wahls, J. Morrison, T. Zickuhr, D. Levy, and M. Murayama. Grid quality and resolution issues from the Drag Prediction Workshop series. *AIAA Journal of Aircraft*, 46(3):935–950, 2009.

[50]4^{th} AIAA CFD Drag Prediction Workshop. http://aaac.larc.nasa.gov/tsab/cfdlarc/aiaa−dpw/, dpw@cessna.textron.com, San Antonio, TX, June 2009.

[51]J. C. Vassberg, M. A. DeHaan, S. M. Rivers, and R. A. Wahls. Development of a Common Research Model for applied CFD validation studies. *AIAA Paper 2008-6919*, 26^{th} AIAA Applied Aerodynamics Conference, Hawaii, HI, August 2008.

[52]M. Rivers and A. Dittberner. Experimental investigations of the NASA Common Research Model. *AIAA Paper 2010-4218*, 28^{th} AIAA Applied Aerodynamics Conference, Chicago, IL, June 2010.

[53]J. H. Morrison. Statistical analysis of CFD solutions from the Fourth AIAA Drag Prediction Workshop. *AIAA Paper 2010-4673*, 28^{th} AIAA Applied Aerodynamics Conference, Chicago, IL, June 2010.

[54]A. J. Sclafani, J. C. Vassberg, C. Rumsey, M. A. DeHaan, and T. H. Pulliam. Drag prediction for the NASA CRM wing/body/tail using CFL3D and OVERFLOW on an overset mesh. *AIAA Paper 2010-4219*, 28^{th} AIAA Applied Aerodynamics Conference, Chicago, IL, June 2010.

[55]D. Hue, M. Gazaix, and S. Esquieu. Computational drag and moment prediction of the DPW4 configuration with elsA. *AIAA Paper 2010-4220*, 28^{th} AIAA Applied Aerodynamics Conference, Chicago, IL, June 2010.

[56]M. Mani, B. J. Rider, A. J. Sclafani, C. Winkler, J. C. Vassberg, A. J. Dorgan, A. Cary, and E. N. Tinoco. RANS technology for transonic drag prediction; a Boeing perspective of the 4^{th} Drag Prediction Workshop. *AIAA Paper 2010-4221*, 28^{th} AIAA Applied Aerodynamics Conference, Chicago, IL, June 2010.

[57]K. Yamamoto, K. Tanaka, and M. Murayama. Comparison study of drag prediction for the 4^{th} CFD Drag Prediction Workshop using structured and unstructured mesh methods. *AIAA Paper 2010-4222*, 28^{th} AIAA Applied Aerodynamics Conference, Chicago, IL, June 2010.

[58]O. Brodersen, S. Crippa, B. Eisfeld, S. Keye, and S. Geisbauer. DLR results for the Fourth AIAA CFD Drag Prediction Workshop. *AIAA Paper 2010-4223*, 28^{th} AIAA Applied Aerodynamics Conference, Chicago, IL, June 2010.

[59]P. Eliasson, S. Peng, and L. Tysell. Computations from the 4^{th} Drag Prediction Workshop using the Edge solver. *AIAA Paper 2010-4548*, 28^{th} AIAA Applied Aerodynamics Conference, Chicago, IL, June 2010.

[60]G. Li and Z. Zhou. Validation of a multigrid-based Navier-Stokes solver for transonic flows. *AIAA Paper 2010-4549*, 28^{th} AIAA Applied Aerodynamics Conference, Chicago, IL, June 2010.

[61]D. J. Mavriplis and M. Long. NSU3D results for the Fourth AIAA Drag Prediction Workshop. *AIAA Paper 2010-4550*, 28^{th} AIAA Applied Aerodynamics Conference, Chicago, IL, June 2010.

[62]E. Lee-Rausch, E. Hammond, E. Nielsen, S. Pirzadeh, and C. Rumsey. Application of the FUN3D unstructured-grid Navier-Stokes solver to the 4^{th} AIAA Drag Prediction Workshop cases. *AIAA Paper 2010-4551*, 28^{th} AIAA Applied Aerodynamics Conference, Chicago, IL, June 2010.

[63]J. Vos, S. Sanchi, A. Gehri, and P. Stephani. DPW4 results using different grids, including near-field/far-field drag analysis. *AIAA Paper 2010-4552*, 28^{th} AIAA Applied Aerodynamics Conference, Chicago, IL, June 2010.

[64]A. Hashimoto, P. Lahur, K. Murakami, and T. Aoyama. Validation of fully automatic grid generation method on aircraft drag prediction. *AIAA Paper 2010-4669*, 28^{th} AIAA Applied Aerodynamics Conference, Chicago, IL, June 2010.

[65]L. Temmerman and C. Hirsch. Simulations of the CRM configuration on unstructured hexahedral grids: Lessons learned from the DPW-4 workshop. *AIAA Paper 2010-4670*, 28^{th} AIAA Applied Aerodynamics Conference, Chicago, IL, June 2010.

[66]M. Chaffin and D. Levy. Comparison of viscous grid layer growth rate of unstructured grids on CFD Drag Prediction Workshop results. *AIAA Paper 2010-4671*, 28^{th} AIAA Applied Aerodynamics Conference, Chicago, IL, June 2010.

[67]S. Crippa. Application of novel hybrid mesh generation methodologies for improved unstructured CFD simulations. *AIAA Paper 2010-4672*, 28^{th} AIAA Applied Aerodynamics Conference, Chicago, IL, June 2010.

[68]T. J. Baker. Mesh generation: Art or science? *Progress in Aerospace Sciences*, 41:29–63, 2005.

[69]M. D. Salas. Digital flight: The last CFD aeronautical grand challenge. *Journal of Scientific Computing, Vol. 28, No. 213*, pages 479–505, September 2006.

[70]G. M. Gatlin, S. M. Rivers, S. L. Goodliff, R. Rudnik, and M. Sitzmann. Experimental investigation of the DLR-F6 transport configuration in the National Transonic Facility. *AIAA Paper 2008-6917*, 26^{th} AIAA Applied Aerodynamics Conference, Hawaii, HI, August 2008.

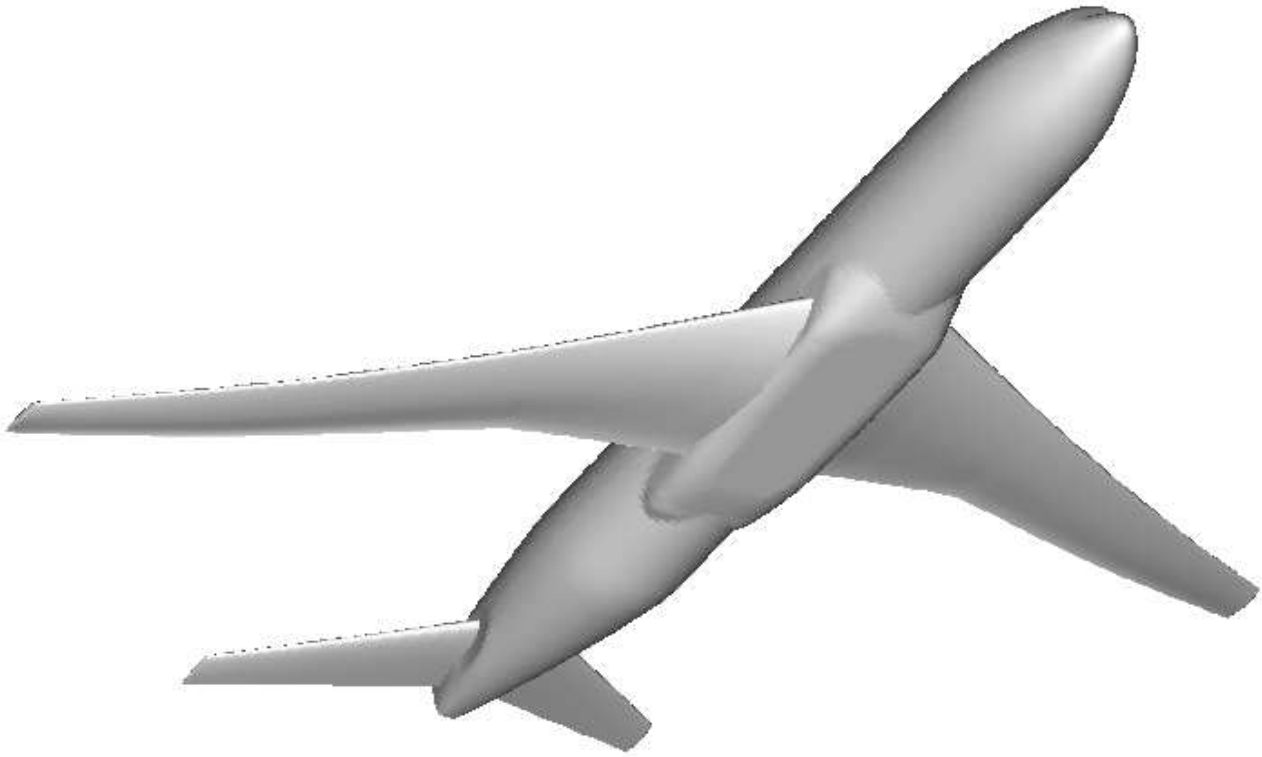

Figure 1. CRM Wing-Body-Horizontal (WBH) Configuration.

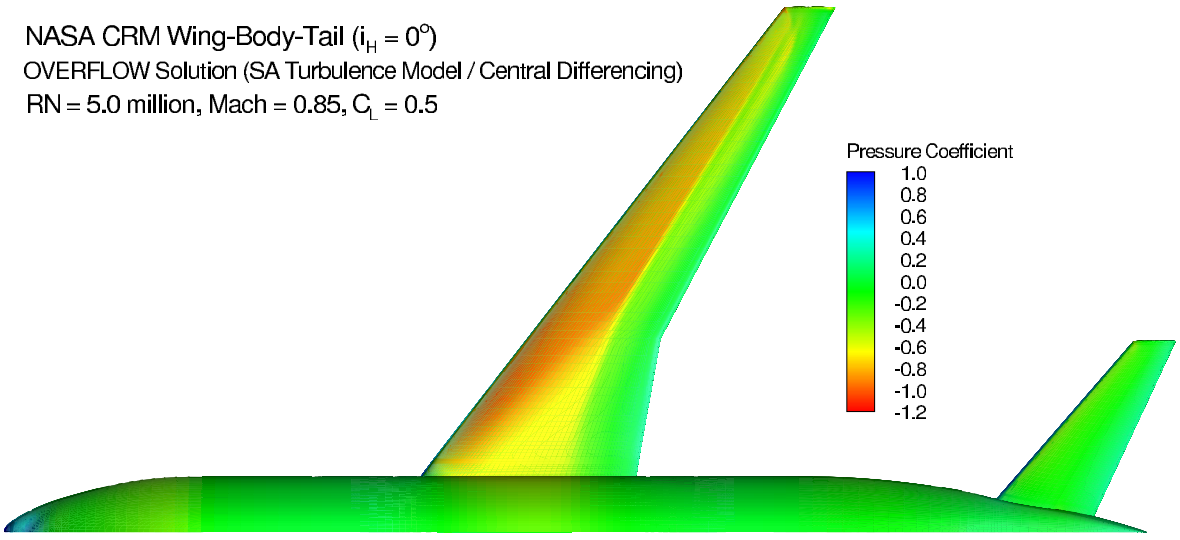

Figure 2. Upper-Surface Pressures on the CRM WBH: $M = 0.85$, $C_L = 0.5$, $Re = 5\ million$.

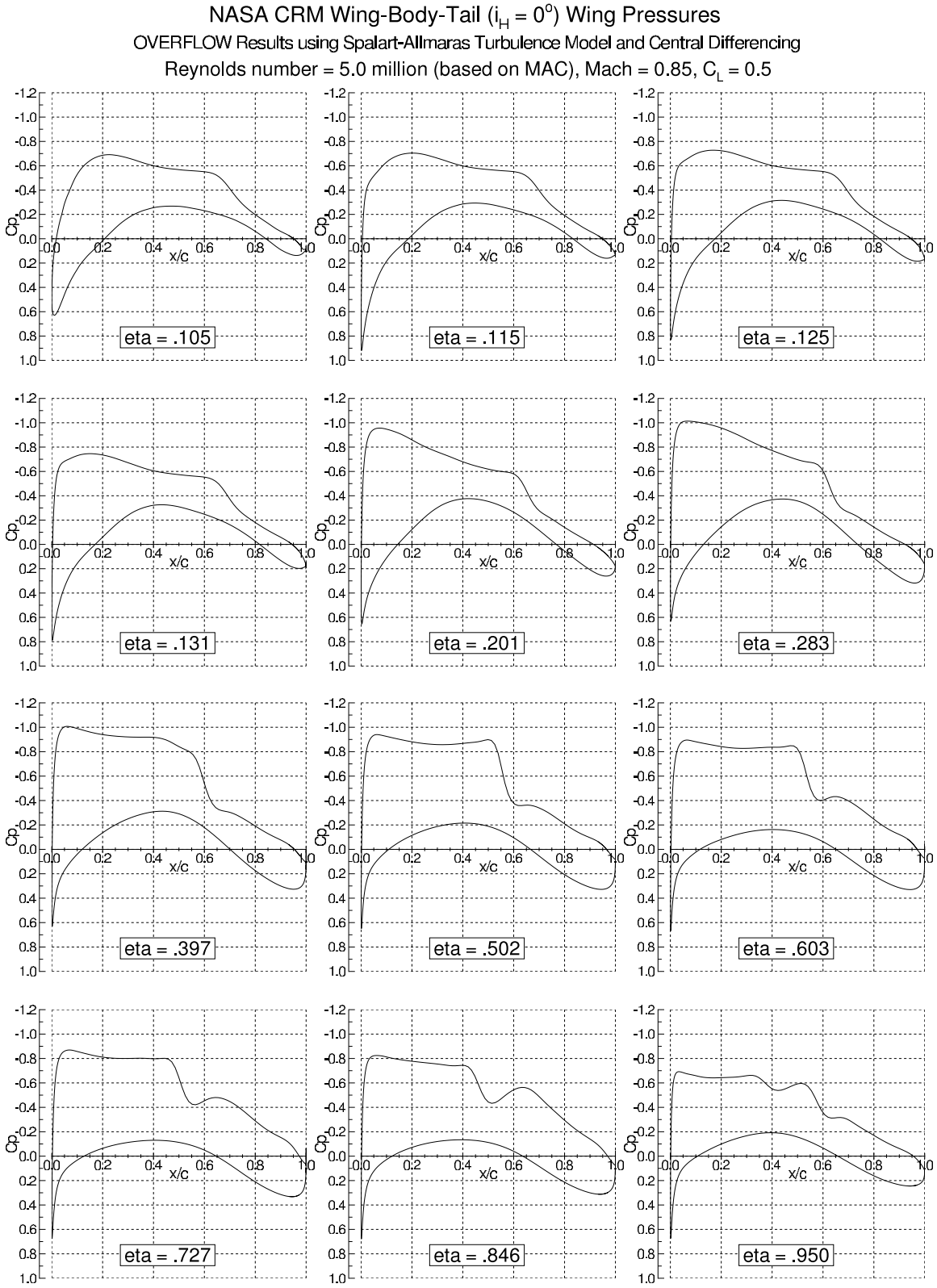

Figure 3. Pressure Distributions on the CRM WBH: $M = 0.85$, $C_L = 0.5$, $Re = 5$ *million*.

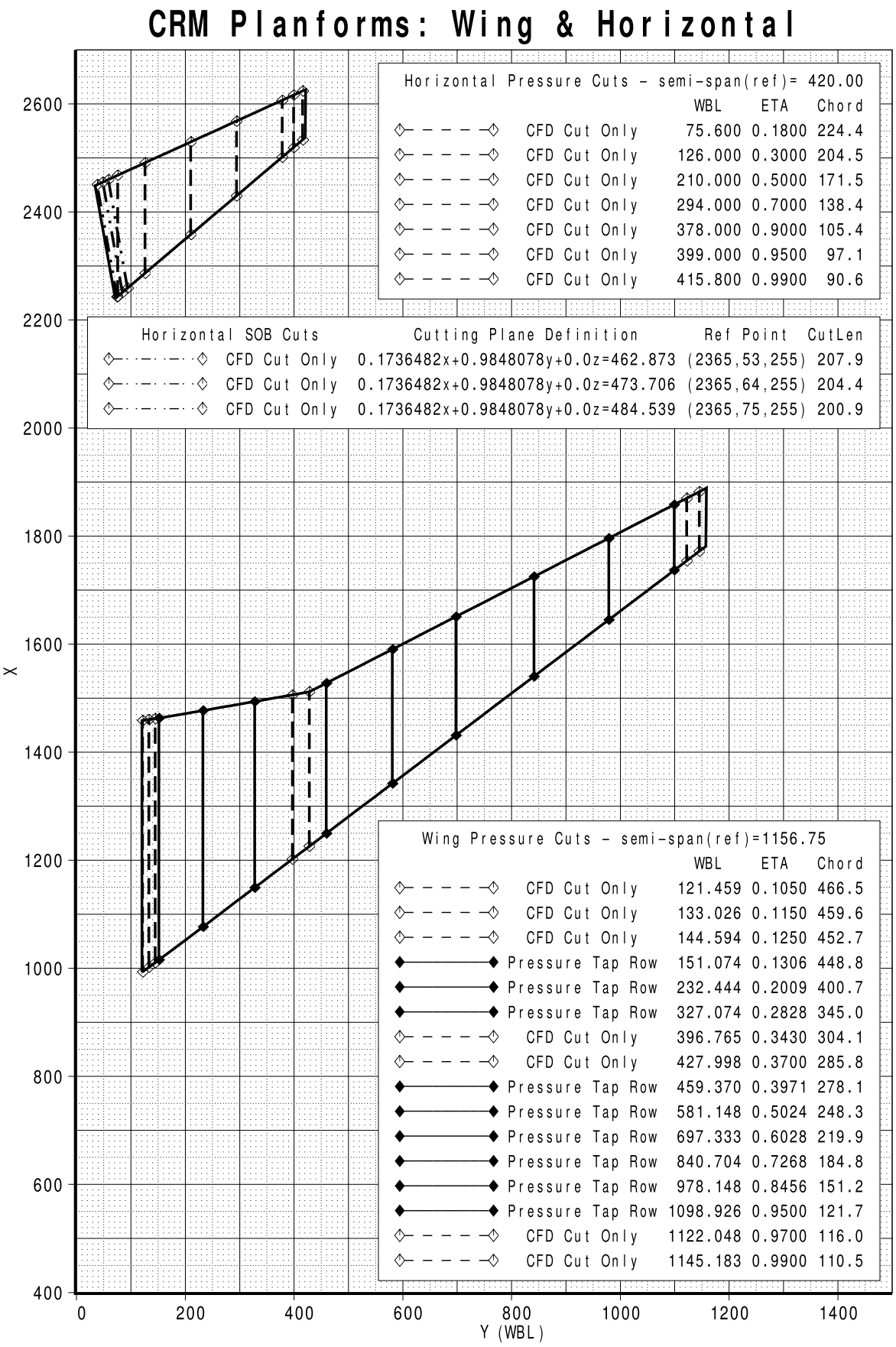

Figure 4. Locations of Pressure Cuts on the CRM WBH.

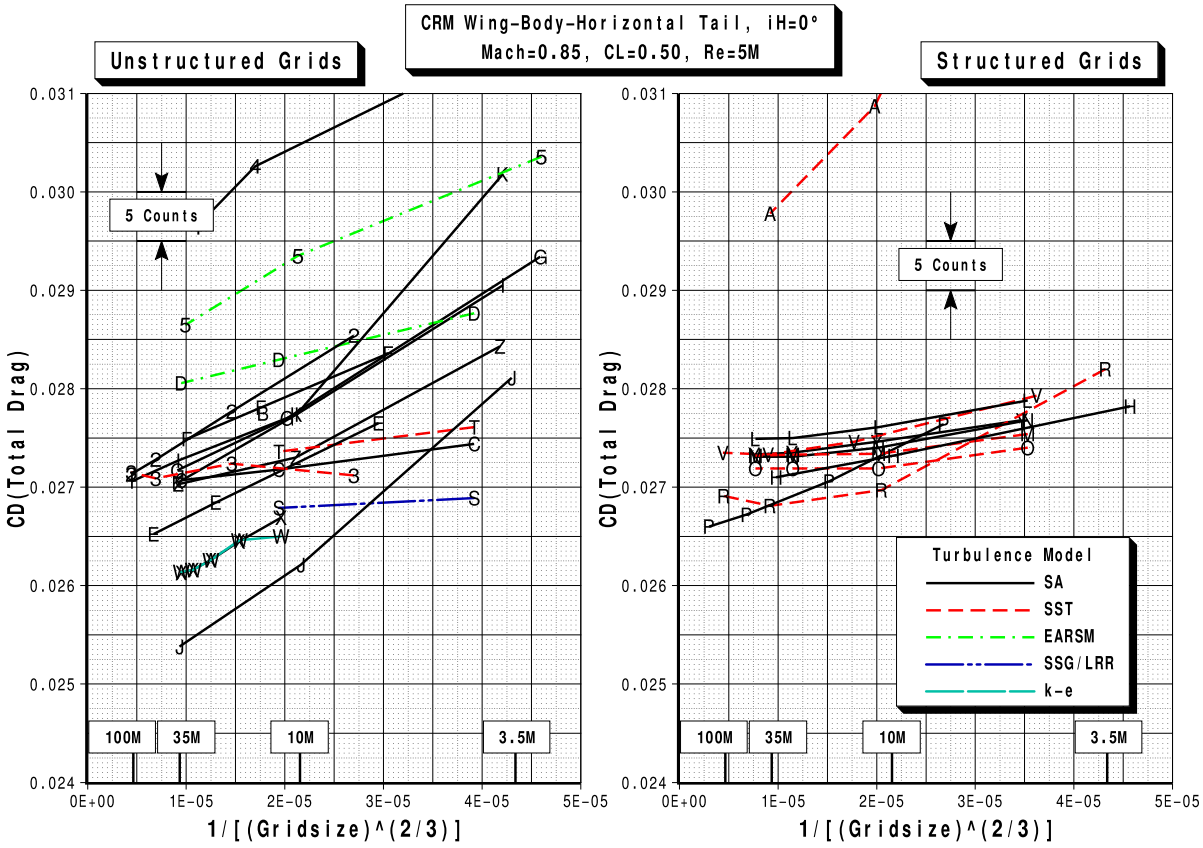

Figure 5. Case 1a Grid Convergence on Total Drag: $M = 0.85$, $C_L = 0.5$, $Re = 5$ *million*.

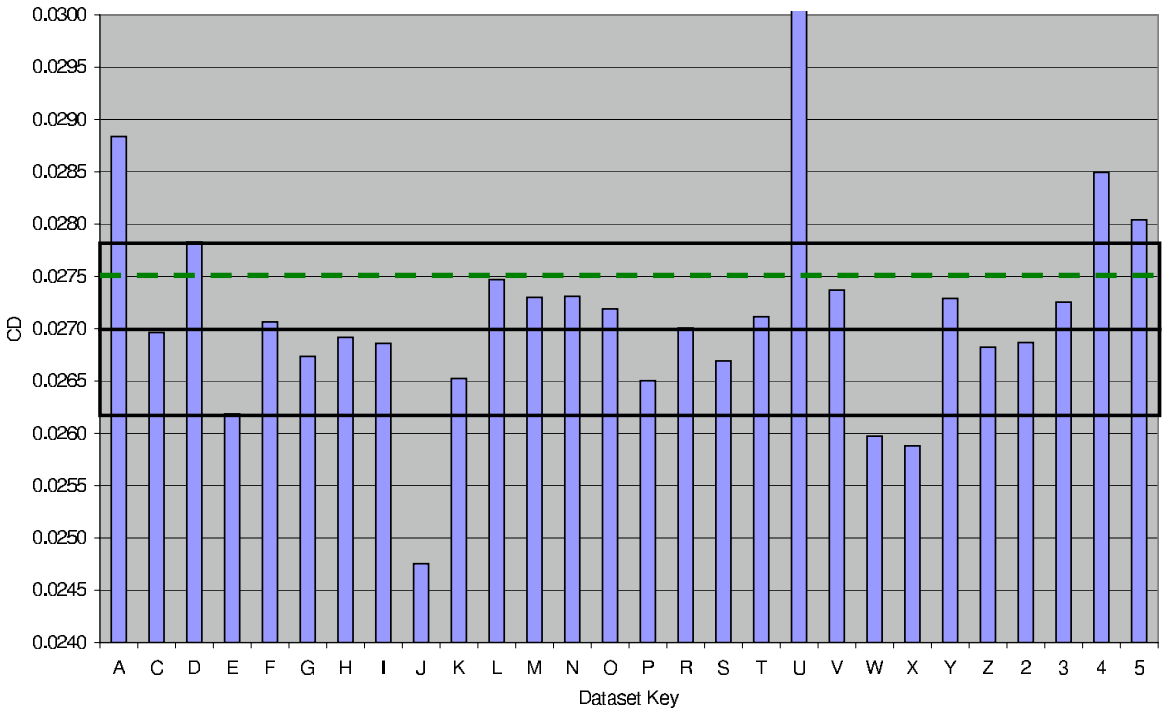

Figure 6. Case 1a Continuum Estimates of Total Drag: $M = 0.85$, $C_L = 0.5$, $Re = 5$ *million*.

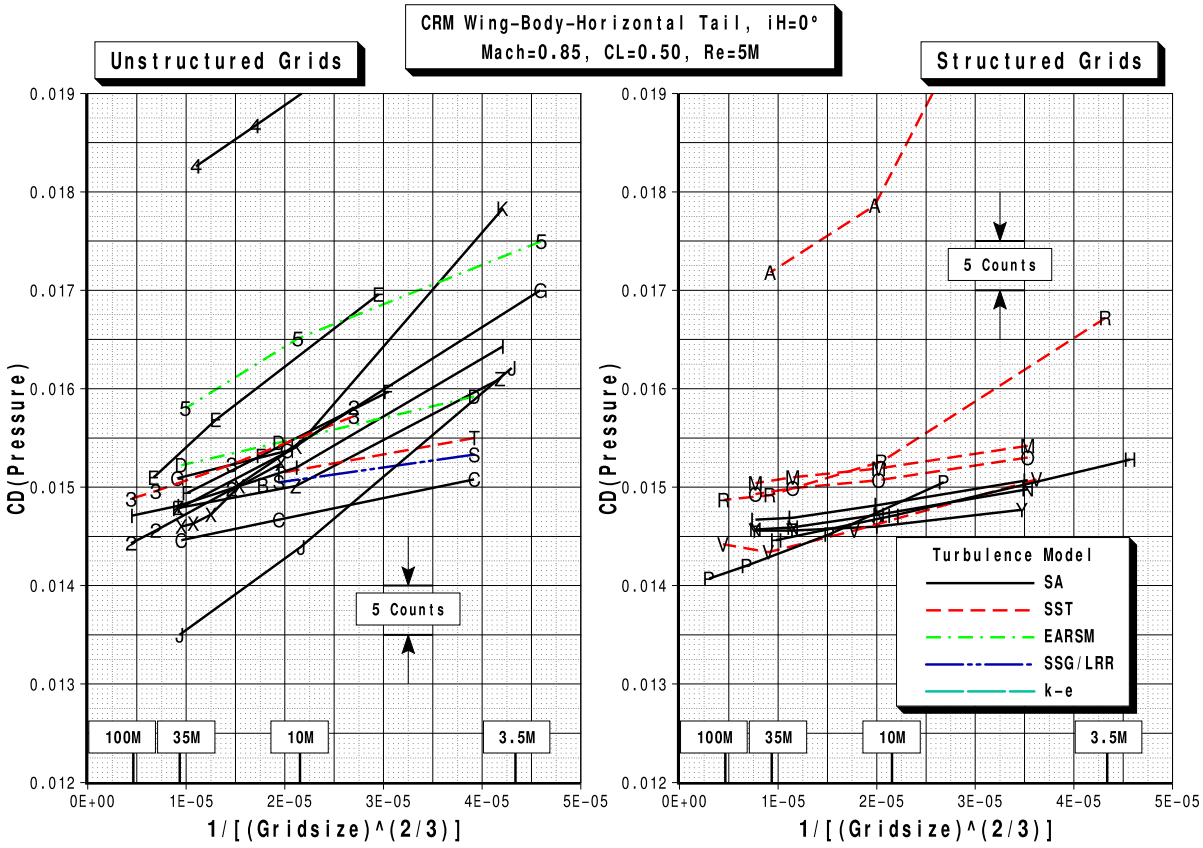

Figure 7. Case 1a Grid Convergence on Pressure Drag: $M = 0.85$, $C_L = 0.5$, $Re = 5$ *million*.

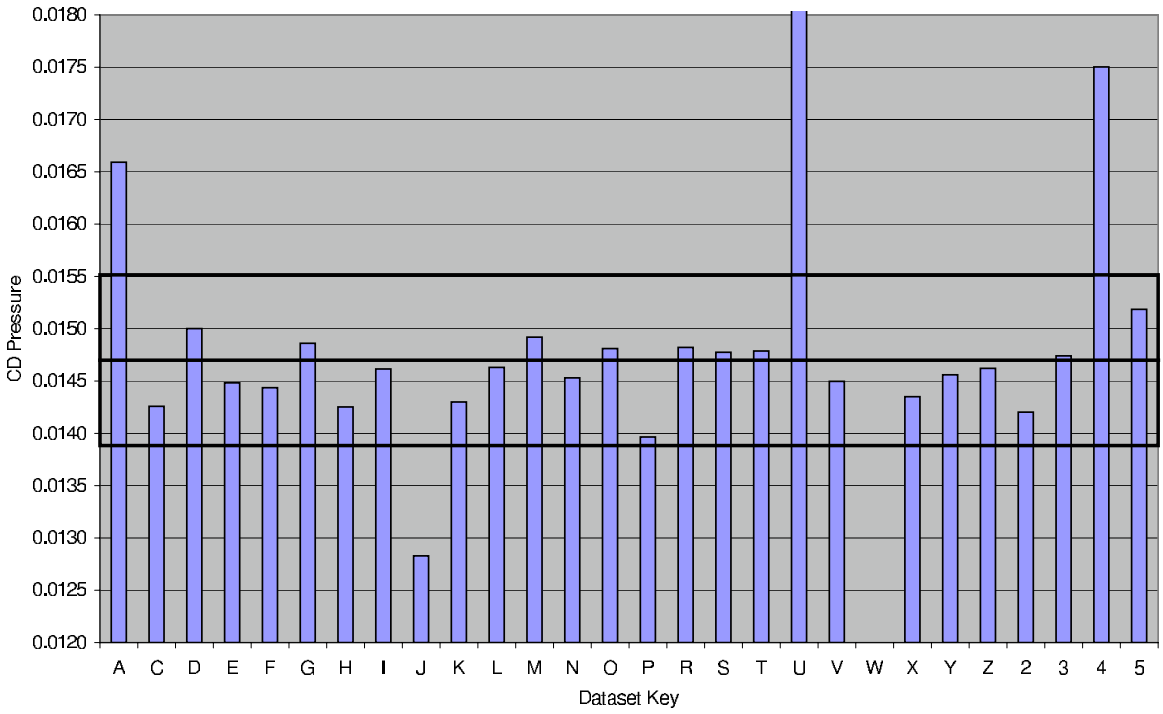

Figure 8. Case 1a Continuum Estimates of Pressure Drag: $M = 0.85$, $C_L = 0.5$, $Re = 5$ *million*.

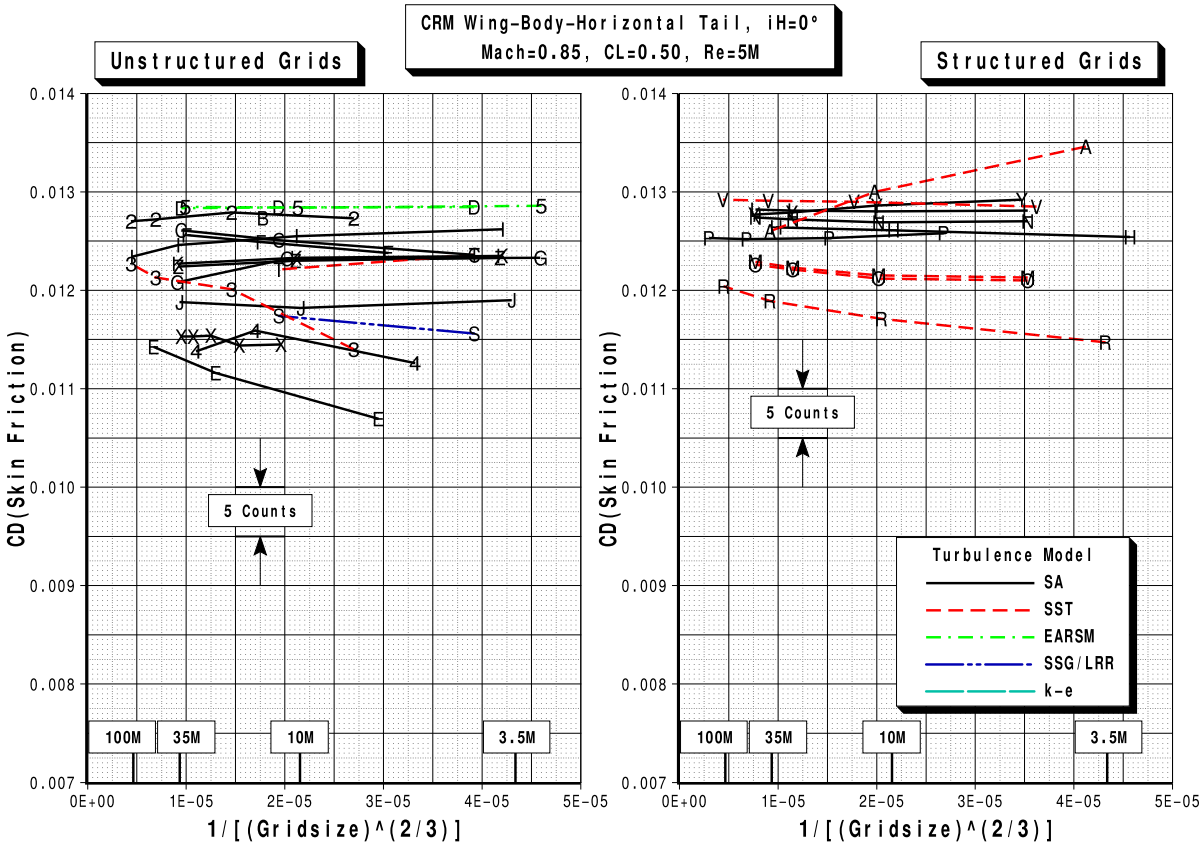

Figure 9. Case 1a Grid Convergence on Skin-Friction Drag: $M = 0.85$, $C_L = 0.5$, $Re = 5$ *million*.

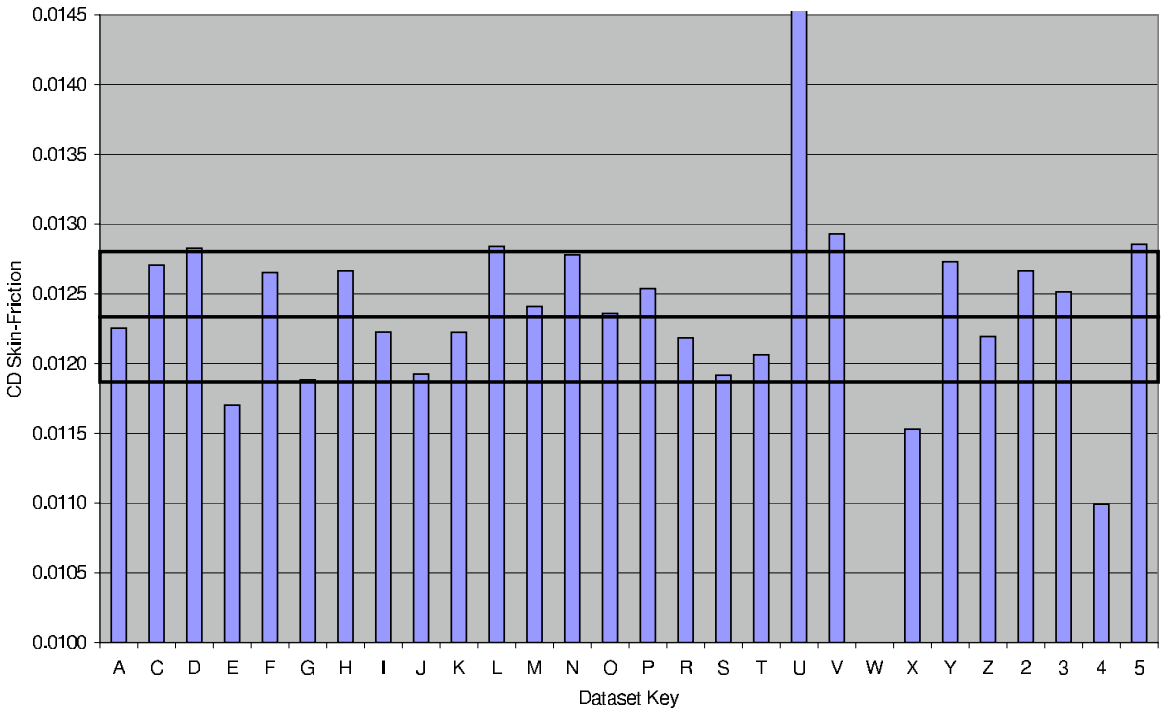

Figure 10. Case 1a Continuum Estimates of Skin-Friction Drag: $M = 0.85$, $C_L = 0.5$, $Re = 5$ *million*.

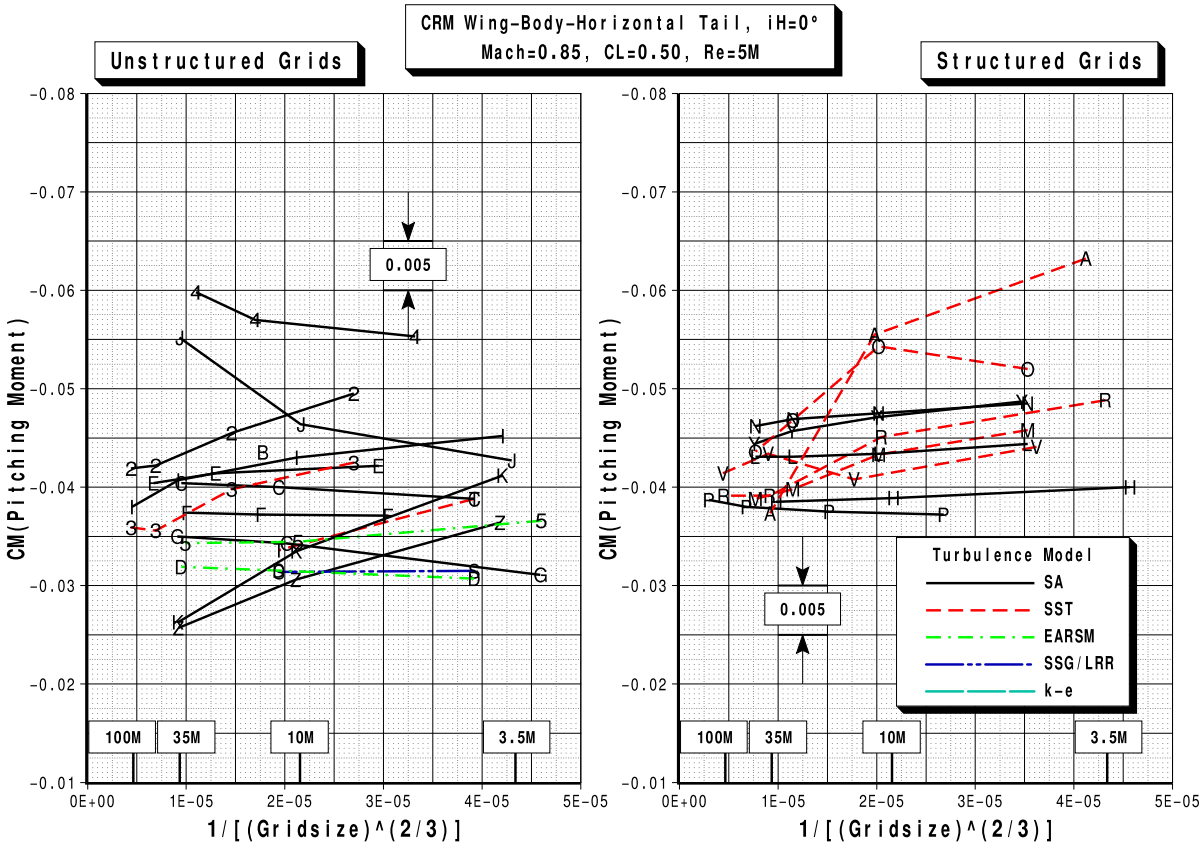

Figure 11. Case 1a Grid Convergence on Pitching Moment: $M = 0.85$, $C_L = 0.5$, $Re = 5$ *million*.

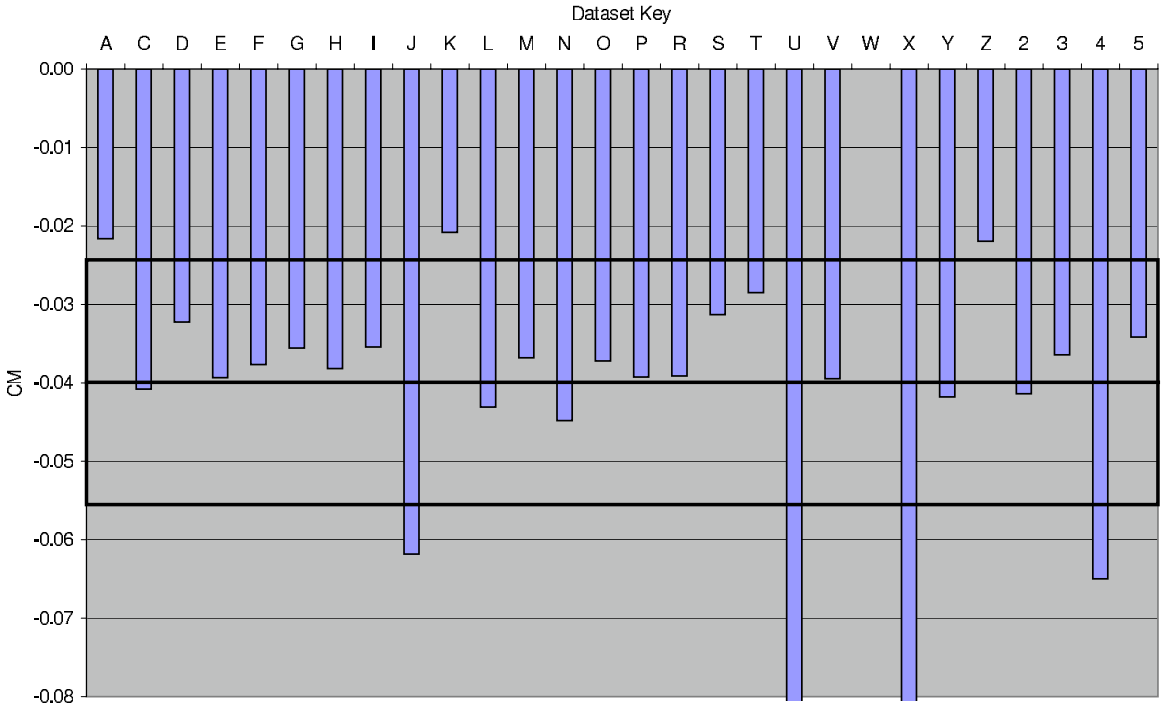

Figure 12. Case 1a Continuum Estimates of Pitching-Moment: $M = 0.85$, $C_L = 0.5$, $Re = 5$ *million*.

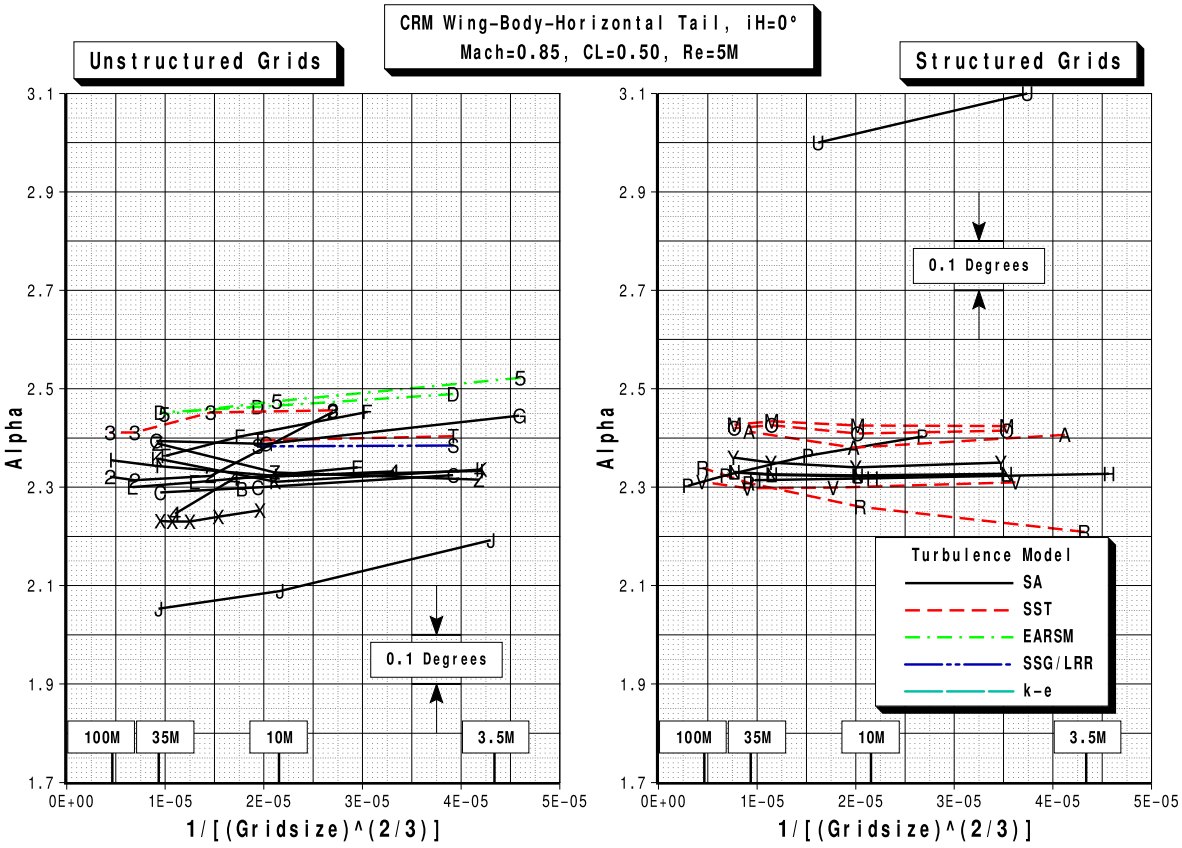

Figure 13. Case 1a Grid Convergence on Alpha: $M = 0.85$, $C_L = 0.5$, $Re = 5$ *million*.

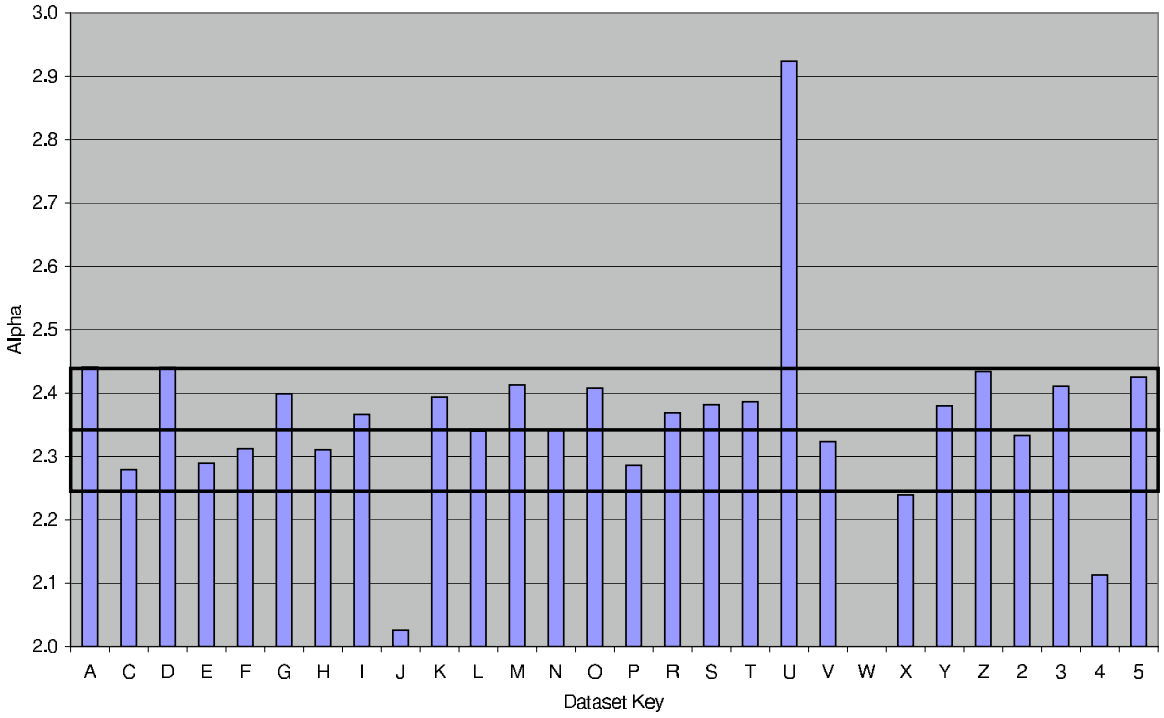

Figure 14. Case 1a Continuum Estimates of Alpha: $M = 0.85$, $C_L = 0.5$, $Re = 5$ *million*.

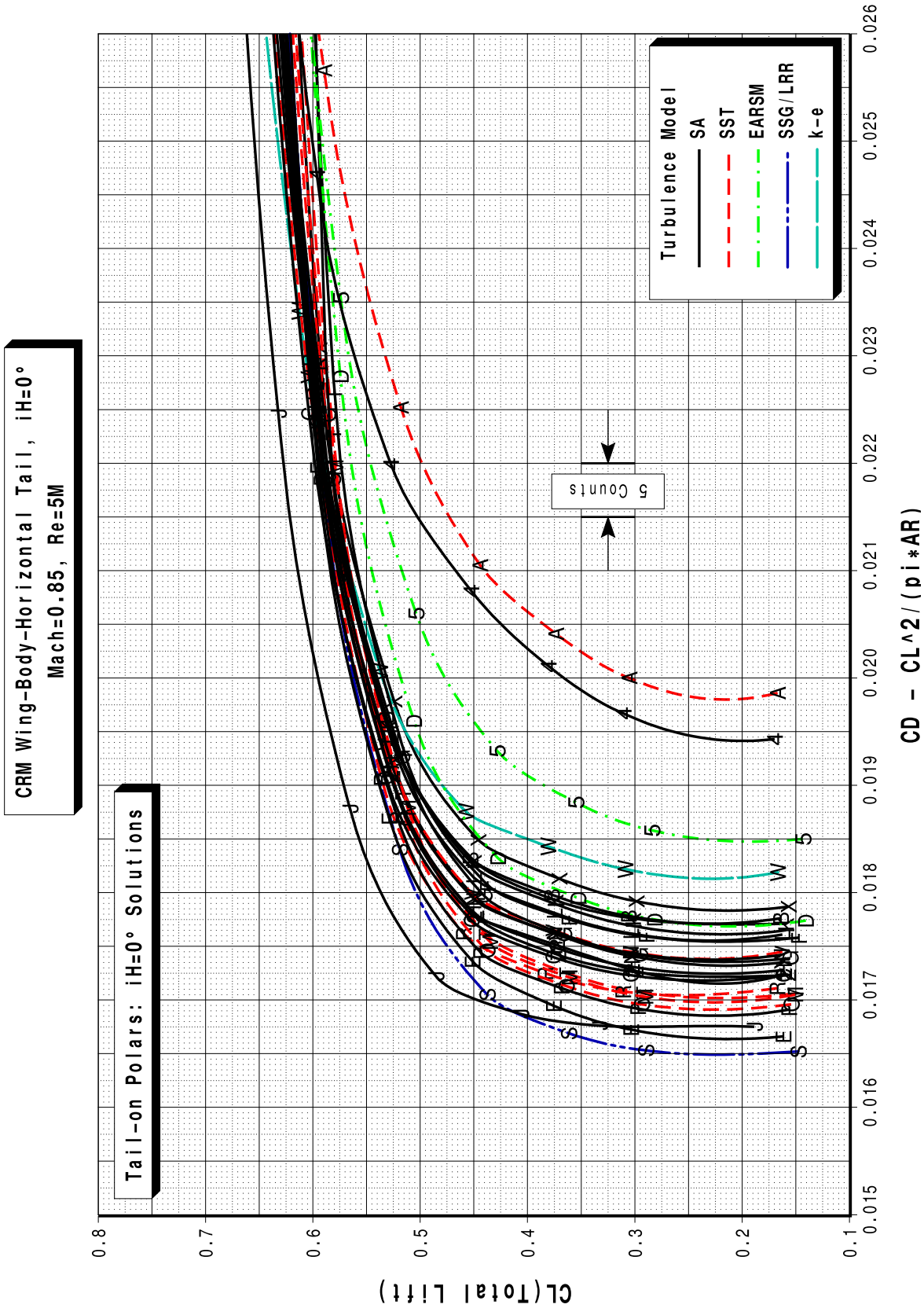

Figure 15. Case 1b Idealized Profile Drag Polars: $M = 0.85$, $C_L = 0.5$, $Re = 5$ *million*, $iH = 0°$.

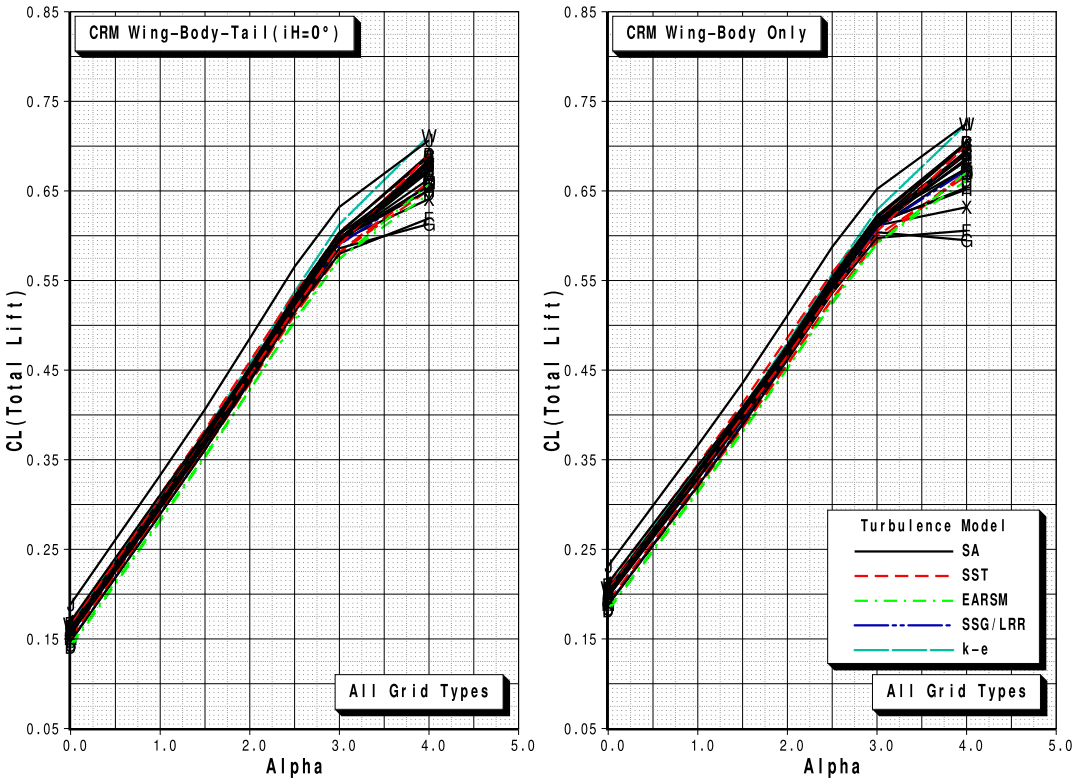

Figure 16. Case 1b Lift Curves: $M = 0.85$, $C_L = 0.5$, $Re = 5\ million$, $iH = 0°$.

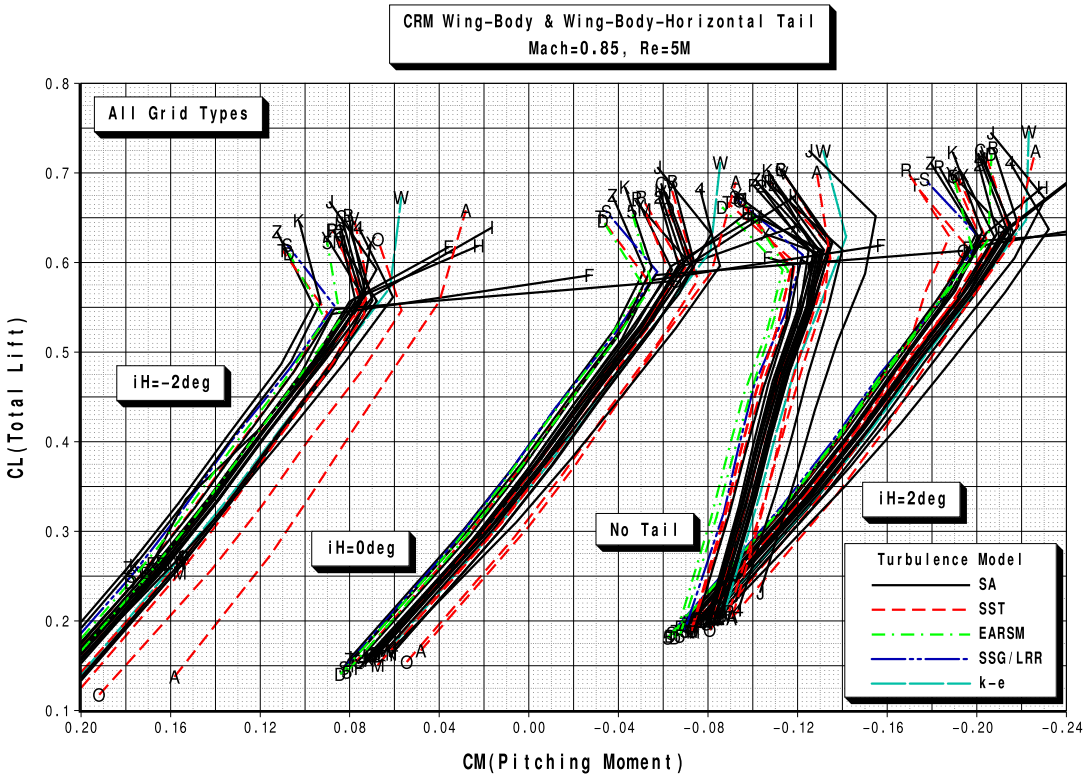

Figure 17. Case 1b Pitching Moment Curves.

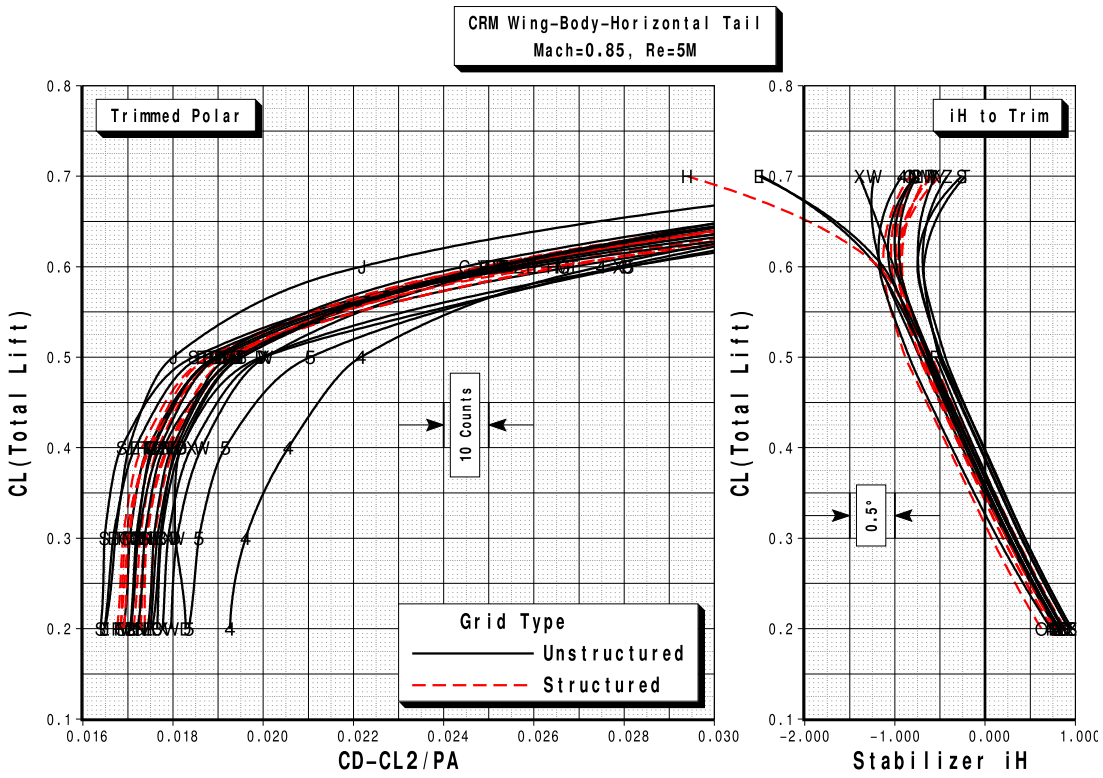

Figure 18. Case 1b Trimmed Drag Polars and Trimmed Horizontal-Tail Settings: $M = 0.85$, $C_L = 0.5$, $Re = 5$ *million*.

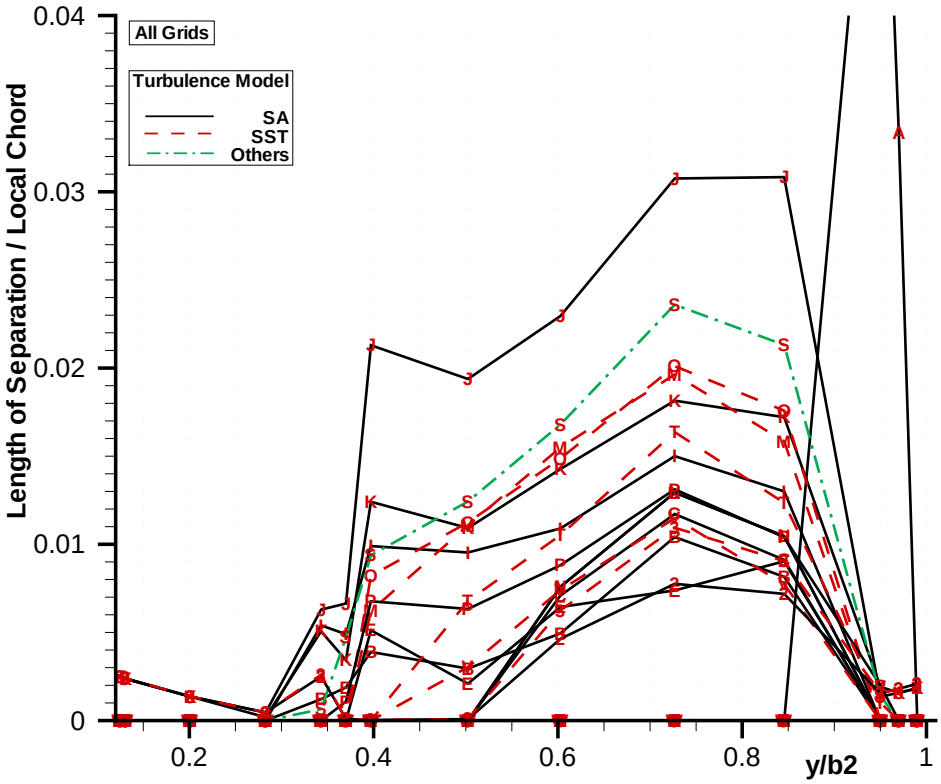

Figure 19. Case 1 Trailing-Edge Separation: $M = 0.85$, $C_L = 0.5$, $Re = 5$ *million*.

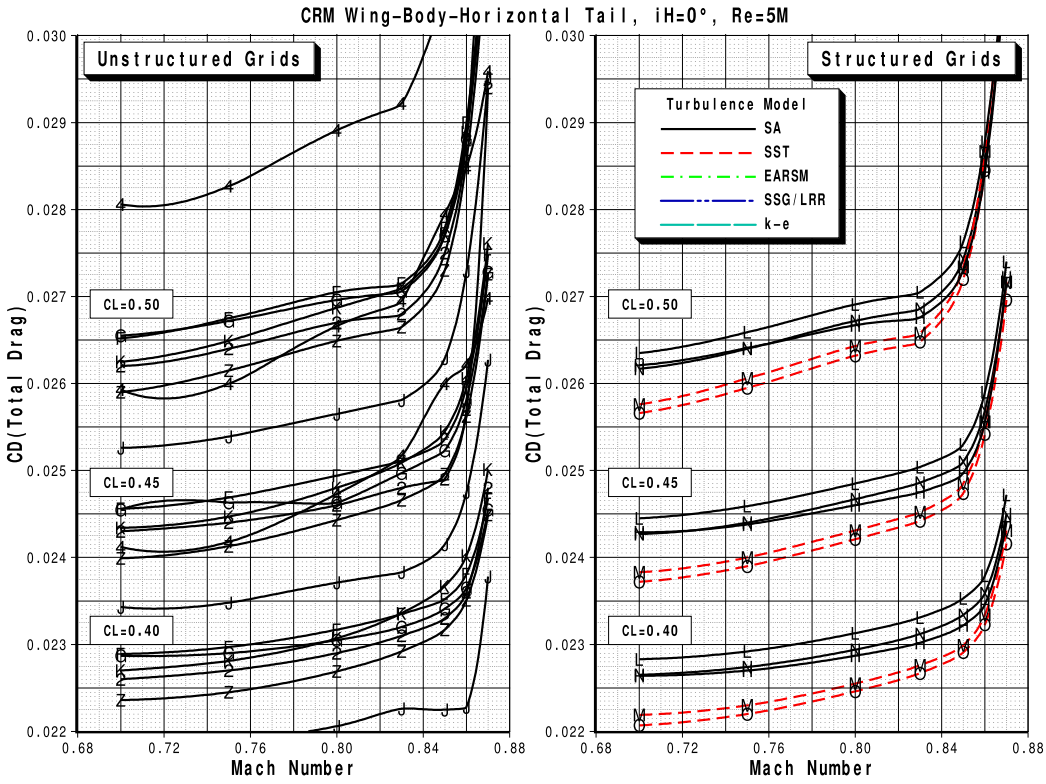

Figure 20. Case 2 Drag-Rise Curves.

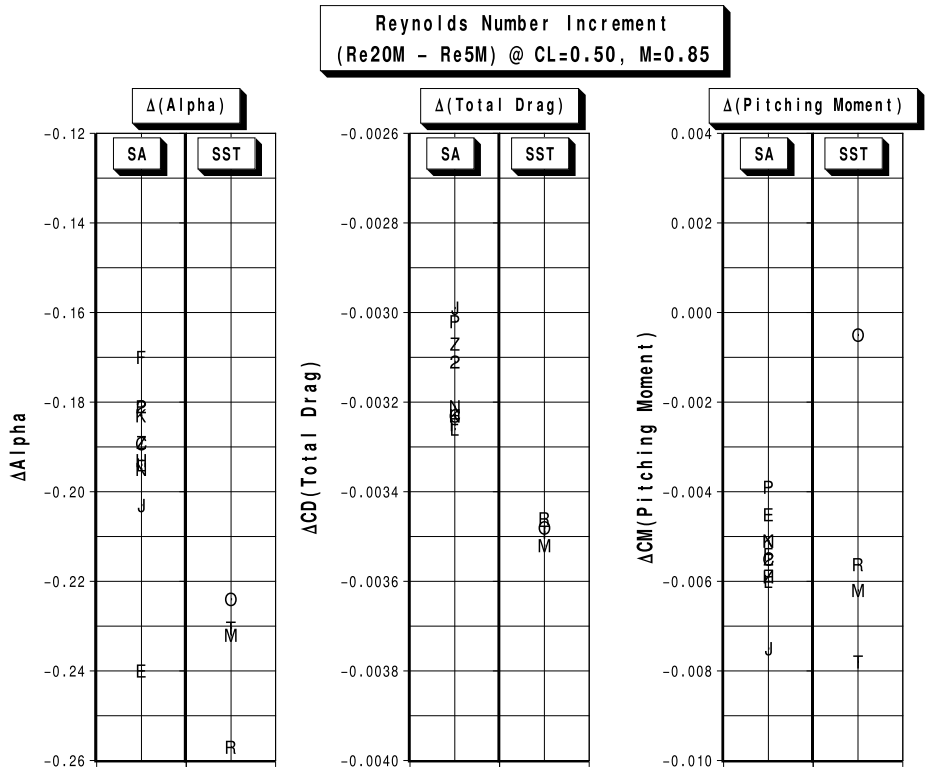

Figure 21. Case 3 Reynolds-number study: $M = 0.85$, $C_L = 0.5$, $Re = [5, 20]$ *million*.